TEMPERATURE INDEX MODELING OF THE KAHILTNA GLACIER:

COMPARISON TO MULTIPLE FIELD

AND GEODETIC MASS BALANCE DATASETS

By

Joanna C. Young

RECOMMENDED:

Dr. Regine Hock

Dr. Roman Motyka

Dr. Anthony Arendt
Advisory Committee Chair

Dr. Paul McCarthy
Chair, Department of Geology and Geophysics

APPROVED:

Dr. Paul Layer
Dean, College of Natural Science and Mathematics

Dr. John Eichelberger
Dean of the Graduate School

December 16, 2013
Date

TEMPERATURE INDEX MODELING OF THE KAHILTNA GLACIER: COMPARISON TO MULTIPLE FIELD AND GEODETIC MASS BALANCE DATASETS

A

THESIS

Presented to the Faculty

of the University of Alaska Fairbanks

in Partial Fulfillment of the Requirements

for the Degree of

MASTER OF SCIENCE

By

Joanna C. Young, B.S., B.A.

Fairbanks, Alaska

December 2013

Abstract

Glaciers of Alaska, USA, and Northwestern Canada are shedding mass at one of the highest rates of any mountain glacier system, with significant impact at the global and local scales. Despite advances in satellite and airborne technologies, fully characterizing the temporal evolution of glacier mass change in individual watersheds remains a challenge. Temperature index modeling is an approach that can be used to expand on sparse ground observations, and that can help bridge the gap between regional and individual watershed estimates of the time series of glacier mass change. Here we present a study on temperature index modeling of glacier-wide mass balance for the large Kahiltna Glacier (502 km^2, 270 to 6100 m in elevation) in the Central Alaska Range, using a combination of ground observations and past climate data products. We reproduce mass changes from 1991 to 2011, and assess model performance by comparing our results to several field and remote sensing datasets. First, we compare our results to a 20-year record of mass balance measurements at a National Park Service index site at the glacier's equilibrium line altitude. We find low correlation between index site measurements and modeled glacier-wide balances (R^2 = 0.24), indicating that the index site may not be representative of the glacier-wide mass balance regime. We compare next to glacier-wide mass balances derived from airborne laser altimetry, to assess the model's long-term mass change estimates. We find disagreement between the mean annual balances for 1995 to 2010 (-0.95 $\pm$0.49 m w.e. yr^{-1} from the model versus -0.69 +0.07/-0.08 m w.e. yr^{-1} from laser altimetry). To validate the laser altimetry methods, we then compare estimates from 1951 to 2011 from laser altimetry and digital elevation model differencing, finding close agreement (-0.48 +0.08/-0.09 m w.e. yr^{-1} and -0.41 $\pm$0.26 m w.e. yr^{-1}, respectively), and lending strength to the laser altimetry centerline extrapolation techniques. We also examine estimates derived from regionally-downscaled satellite gravimetry. While gravimetry likely underestimates long-term mass loss for this glacier (-0.36 $\pm$0.13 m w.e. yr^{-1} for 2003 to 2010), it correlates well to individual modeled annual balances (R^2 = 0.72) and to the time series of mass balance at an ablation stake location (R^2 = 0.81). Given ongoing refinements to gravimetry downscaling and geodetic techniques, our results point to the potential for integrating multiple methods to obtain the most information on subannual and long-term mass changes at the basin scale for remote sites such as the Kahiltna Glacier.

Table of Contents

Page

List of Figures

Page

Page

List of Tables

Page

Acknowledgements

I would first and foremost like to thank my advisor, Dr. Anthony Arendt, fellow Canadian (which must be why we get along so well). He has been an excellent mentor, pushing me in the ways that I needed to be challenged, and letting me have freedom in the areas that I wanted to explore. Anthony has put up with a lot! His patient manner of encouraging my progress is testament to his ability to focus even the shortest of attention spans. But at the same time, I can always count on him to promote opportunities for adventure and growth. I have developed hugely as a scientist and a communicator under his guidance, and am leaving this degree with a broader skill set than I ever anticipated when I came to be his student at this small university in the middle of the sub-Arctic taiga. Which is why I am excited to continue on to a PhD here at UAF, still under his mentorship.

I would like to thank my committee members, Dr. Regine Hock and Dr. Roman Motyka. Regine has provided invaluable assistance with the modeling aspects of this work, with interpretation of results, and with making sure I'm always ready to answer the scary but important question: "So... why is this interesting?" She also keeps the Glaciers Group cohesive by organizing seminars and hosted events, throwing great parties, and baking great cakes (even if they tend not to be vegan). Roman contributed valuable advice for navigating the can of worms that is DEM differencing with terrible maps, and provided input for improved writing. I have yet to be in the field with him, but hope to one day soon – his reputation as a gourmet field chef precedes him.

Thank you to also to my funding agencies: The National Park Service (who sponsored me through the George Melendez Wright Climate Change Fellowship, and through grant number H9911080028), the Center for Global Change and Arctic System Research (who awarded me a Global Change Student Research Grant), the Cooperative Institute for Alaska Research, the Alaska Climate Science Center, the National Pacific Research Board, and the National Science Foundation (EAR-0911764).

The Glaciers Group at the GI has played no small part in the writing of this thesis and in my development as a scientist. Thank you to all of the research technicians and post-docs for their passion for ice, and for hilarious water-cooler banter. Thank you also to the professors, faculty and emeritus for having an open-door policy, for being inspired by our incredible subject and geographic setting, and for going to every length to insist that we

must all sit on the 4th floor of the GI together. It wouldn't work any other way.

My fellow glaciology graduate students have provided a tight network of friends and at-the-ready resources, full of knowledge, experience, and tips – how to do things well, how to do them efficiently, or how not to do them and convince your committee that you shouldn't have to. I learned as much from them during our day-to-day interactions as I did from any textbook or course. Thanks to you all. Despite sitting together in our cubicle maze for so long, reading the same papers, trying to figure out the same Matlab intricacies, I am really excited to see how each of us takes this shared experience and does something completely different with it.

A special thank you to Sam Herreid, too, resident undergraduate glaciologist extraordinaire, who admittedly taught me as much about how to be a good graduate student as I taught him about how to be a good undergrad. I owe him a huge debt of gratitude, and a big bottle of whisky.

Launching the Girls on Ice Alaska program has been a major item on my list of accomplishments here at UAF, so thank you to Barbara and Marijke for helping make it a reality – I still can't believe we did it! – and to Erin for being our patient and motivating mentor. Erin has created a truly inspiring program, and I am excited to be a part of its continuing evolution during my future years at UAF. I'm also looking forward to Barbara's and Marijke's annual trips back to Fairbanks from Switzerland so that they can instruct the course with me! (Right?)

Thanks also to all of the other faculty and grad student friends at the GI. Many pints have been shared, either on Friday nights at the Pub or not-so-secretly late at night in our cubes. I think we all have to admit that though we always complained about the grueling hours of our work, we sometimes stayed late just because we enjoyed each other's company.

For the friends and roommates who have made Fairbanks a great place to live, the chalet a real home and family, and the state of Alaska a giant playground, you have no idea how much you've meant! I owe this degree as much to you as to anyone else, because you have kept me sane through the deadlines and the winter cold spells, and made staying here for another round an easy decision. The community here is really unbelievable. You all know who you are – please don't make me list everyone by name, I will start blushing and you

will laugh! I can't wait to have more absolutely epic chalet parties, Sunday brunches with mimosas, and Alaska wilderness adventures together.

And of course, a huge thank you is owed to my family members, who have all played a very large supporting role in the background. I am eternally fortunate to have followed in the footsteps of two very brilliant scientist sisters, Dr. Young and Dr. Young (i.e. Hilary and Carolyn). The two of them navigated all of the challenges of graduate school before I did, so that I knew how to watch out for both the obstacles and the opportunities. Thanks so much to both of you for, yet again, letting me reap the benefits of being a little sister. All my love also goes to Jeff and Steve, my new brothas-from-anotha-motha, and to my little niece Clara, who is an amazing new excuse to get home to Canada as much as I can.

And finally, thank you so much to my parents, who have always supported my decisions and urged me to do big things. They have tolerated, with empathy and encouragement, dozens of late-night e-mails filled with stress and uncertainty, half-days of our family get-togethers lost to my catching up on sleep, and three daughters who have made financially irresponsible career choices that must be difficult to explain to their friends. And they love us for it – how crazy! I think that if they were not such big adventurers themselves, embarking on new challenges well into their (so-called) retirement, I would not be so motivated to do wild and undeniably rewarding things. Like move to Alaska to live in the woods, ski to school, and study ice.

Chapter 1

Introduction

Glaciers of Alaska, USA, and Northwestern Canada (hereafter called Alaska glaciers for brevity) are shedding mass at one of the highest rates of any mountain glacier system globally (Arendt and others, 2002; Larsen and others, 2007; Meier and others, 2007; Wu and others, 2010; Berthier and others, 2010; Gardner and others, 2013). These mass changes have significant impacts at both global and regional scales. Globally, Alaska glaciers are one of the greatest contributors to eustatic sea-level rise, currently contributing nearly as much freshwater to the rising oceans as the Greenland Ice Sheet (Wu and others, 2010; Berthier and others, 2010; Gardner and others, 2013). At the regional scale, the rapid loss of glacier ice along the Gulf of Alaska over the past 150 years has significantly increased rates of crustal uplift (Sato and others, 2012). Also, melt input from Alaska glaciers, which constitutes nearly half of the total annual land-to-ocean freshwater flux into the Gulf of Alaska (Neal and others, 2010), is largely responsible for driving the Alaska Coastal Current, which delivers nutrients and freshwater along the coast (Royer, 1981). Current estimates attribute 10% of this flux to glacier mass loss associated with the rapid thinning and retreat of Alaska glaciers (Neal and others, 2010).

At the local scale, there is an increasing need for a full temporal characterization of glacier mass balance in individual watersheds. Glacier freshwater discharge has been found to play a key role in supporting the rich coastal marine environments characteristic of Southeast Alaska (Hood and Scott, 2008; Hood and others, 2009), affecting critical water properties such as salinity, temperature, and clarity. Changes in glacial melt quantities and timing therefore lead to changes in the biogeochemical properties of these environments (Hood and Berner, 2009), in turn influencing biological abundance and productivity within the aquatic food web. Moreover, glacier melt also provides an important source for hydroelectric power generation at the watershed scale – studies are currently underway to examine the seasonal and long-term mass variations that will affect existing and proposed hydroelectric dams on glacier-fed lakes and rivers in Alaska (Cherry and others, 2010).

To date, knowledge of the large-scale mass changes of Alaska glaciers has come primarily from two different methods: satellite gravimetry, which provides high temporal but low spatial resolution estimates of mass balance, and airborne altimetry, which provides good

regional coverage but no information on annual or subannual changes. At the local scale, despite considerable advances in satellite remote sensing and airborne observation technologies, our ability to characterize glacier discharge in individual watersheds remains a challenge. Typically, ground observations provide the most accurate information on watershed-scale glacier mass variations; however, such measurements are typically sparse for Alaska glaciers due to remoteness, expense or logistical constraints.

Temperature index modeling is an approach that can help bridge the gap between regional and individual watershed estimates of the time series of glacier mass changes and/or meltwater discharge. This method uses air temperature as a proxy for the dominant energetic processes in glacier melt (Hock, 2005), eliminating the need for complicated model physics for energy balance terms. In fact, simple temperature index models often yield mass balance estimates as accurate as their more sophisticated counterparts (Ohmura, 2001). In addition to helping link regional and watershed estimates of mass change, these models provide insights into the physics of glacier systems and what might be controlling their present and future responses to climate.

Recent studies have applied temperature index models to Alaska glaciers at regional scales, with the primary goal of predicting future evolution of Alaska glaciers in a changing climate (Radić and Hock, 2011; Radić and others, 2013). While these models likely characterize the ensemble of Alaska glaciers due to the minimization of model error over a large sample size, mass balance estimates for individual glaciers may have much larger errors. Only a few studies have applied temperature index models to individual catchments in Alaska (Van Beusekom and others, 2010; Rasmussen and others, 2011). Model performance was good for these glaciers due to a detailed mass balance and climate dataset, allowing for robust model calibration.

Here we present a study on modeling glacier-wide mass balance for the Kahiltna Glacier in the Central Alaska Range, commonly known as Denali National Park. The mass balance of this glacier is of interest to several groups. Researchers at Alaska Pacific University have worked to constrain the timing of downglacier re-emergence of human waste deposited along the well-traveled West Buttress climbing route on Denali, and to evaluate potential effects on downstream water quality (Goodwin and others, 2012). Near-surface radar has recently revealed different thermal zones in the glacier, providing information that can

help guide future mass change projections (Gusmeroli and others, 2013). Also, ground-penetrating radar studies have been conducted, with the goal of locating an ice core site for reconstructing a high-latitude, high-altitude climate record spanning the last few centuries (Campbell and others, 2012b,a). For all of these, knowledge of the mass balance variations of the glacier are critical to constraining the quantities of interest.

Mass balance estimates for this glacier are also relevant to researchers with the National Park Service (NPS), who have for decades collaborated with University of Alaska Fairbanks glaciologists to examine glacier mass change within the park as part of their vital signs monitoring plan (MacCluskie and others, 2005). Techniques have included airborne altimetry and mapping methods (Burrows and others, 2011), as well as ground observations (Burrows and Adema, 2011). While there is a relatively broad range of data available for this glacier, no single dataset is currently capable of fully characterizing both long-term and subannual mass variations. Unlike the US Geological Survey benchmark glaciers Gulkana and Wolverine, which have been monitored in detail since 1965 both in terms of mass balance and local meteorological variables, NPS monitoring efforts on the Kahiltna Glacier have been limited to a single mass balance stake first installed in 1991. There are also few local weather stations with which to drive the model over multiple years.

We therefore draw on the strengths of multiple methods to characterize mass changes of the Kahiltna Glacier. We use a temperature index model driven by climate reanalysis data and calibrated to a series of new ground observations, and compare results to independent observations from three remote sensing techniques. Our goal is to determine the extent to which a temperature index model can be used to characterize the past and present mass variations of this large glacier with sparse in-situ data. As part of these investigations, we examine the extent to which the single NPS mass balance stake can be used to represent glacier-wide mass balances over the 20-year measurement period since the monitoring program began (Burrows and Adema, 2011). We assess model performance by comparing calculated mass balance estimates to those from laser altimetry for an overlapping time period. Moreover, we put present mass changes into a broader context via comparison to USGS maps from the 1950s, to investigate whether mass changes have accelerated over time. Finally, we also compare subannual mass variations determined from the model to those from satellite gravimetry, in order to examine the possibility of extracting seasonal information from the latter, which is a relatively new technology.

Results from this study indicate that given limitations in calibrating a mass balance model to a sparse set of ground observations, future efforts at model development would benefit from integrating new airborne and remote sensing technologies to help determine the best mass change estimates for remote and large field sites such as the Kahiltna Glacier.

1.1 Field site

1.1.1 Kahiltna Glacier

Glaciers of the Central Alaska Range cover a surface area of approximately 3790 km^2 (Burrows and others, 2011) of which about 12% lies within the Kahiltna Glacier basin (Figs. 1.1). With a surface area of 502 km^2 and a centerline length of 72 km, the Kahiltna is the largest glacier within the entire Alaska Range. The Alaska Range forms a sweeping orographic barrier to moist weather systems entering inland off the Gulf of Alaska, essentially separating the maritime climate regime from the dry Interior sub-arctic. Glaciers on the south side of the Central Alaska Range are therefore able to grow significantly larger than those on the north. The Kahiltna Glacier flows southward from the summit of Denali (Mount McKinley), covering altitudes between 6100 m at the uppermost reaches to just 270 m above sea level at the terminus.

The Kahiltna is bordered at its upper reaches by the first and third tallest mountains in North America – Denali and Mount Foraker (Fig. 1.2a) – both of which contribute to significant snowfall to the glacier and which deliver heavy avalanching from their steep slopes. Wind also sweeps many of the steep surrounding granite walls clean of snow, redistributing mass to the tributaries and main glacier trunk. These mass inputs can occur at the upper reaches of the glacier on a year-round basis.

On the eastern side of the Kahiltna Glacier, north of the Big Bend, a number of unnamed tributaries flow into the $\sim$3.5 km-wide main trunk. These tributaries lie in steep valleys in the region south of Mount Hunter, in a complex of relatively small but steep mountains known as Little Switzerland. In contrast, such tributaries are conspicuously absent on the west side of the glacier below the Great Icefall (Fig. 1.2a). The reason for this difference remains unknown.

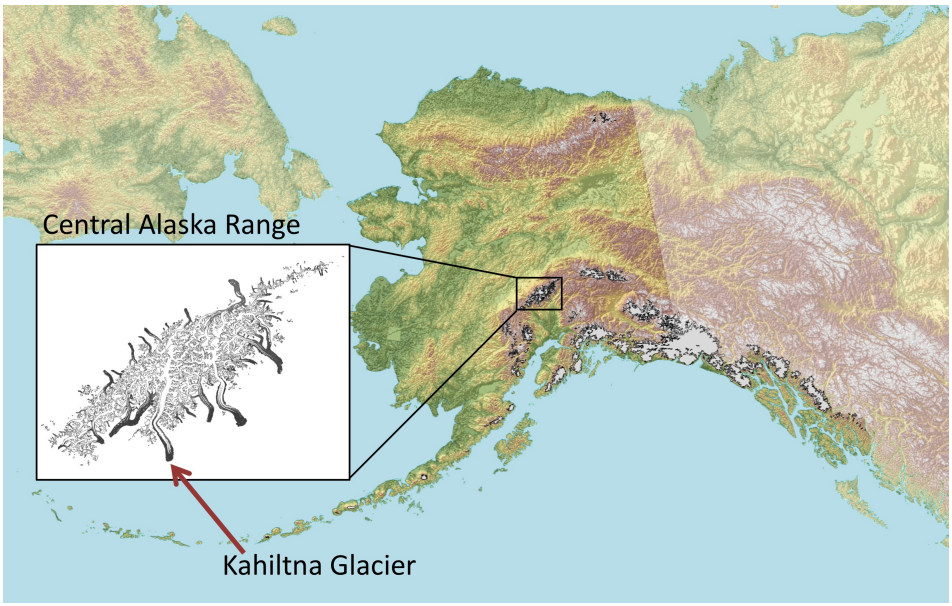

Figure 1.1. Location of the Central Alaska Range within Alaska. Topography is sourced from the National Elevation Dataset digital terrain model, and glacierized areas are shown in light grey with black outlines. Inset: the glacierized portion of the Central Alaska Range and the location of the Kahiltna Glacier, with surficial debris shown in dark grey. Figure by Sam Herreid.

A glacier's equilibrium line altitude (ELA) is defined as the elevation at which, as a long-term average, mass gain from snowfall is equal to mass loss from melt, yielding a mass balance of zero. The average ELA for the Kahiltna Glacier estimated by the NPS for a measurement period spanning from 1991 to 2011 is 1924 m, with a range of 1690 m to 2300 m (Burrows and Adema, 2011). This ELA yields an accumulation-area-ratio of 0.47; Fig. 1.2b).

Evidence from historical photography and a lack of the geomorphological indicators that disclose previous glacier extents (e.g. push moraines beyond the terminus, and various stages of vegetation succession) together suggest that the Kahiltna terminus still remains very near to its Little Ice Age maximum extent. The terminus of the Kahiltna Glacier is largely debris-covered (i.e. 71% covered below 900 m elevation; Fig. 1.2c), as derived from a band ratioing technique applied to Landsat 5/7 scenes (pers. comm. S. Herreid, 2011). This may stabilize the glacier against the rapid retreat seen in many other Alaska glaciers over the past 150 years (Schubert and others, 1998). Dramatic thinning has nevertheless occurred, as is particularly visible in the area around the 'Big Bend,' which is flanked by

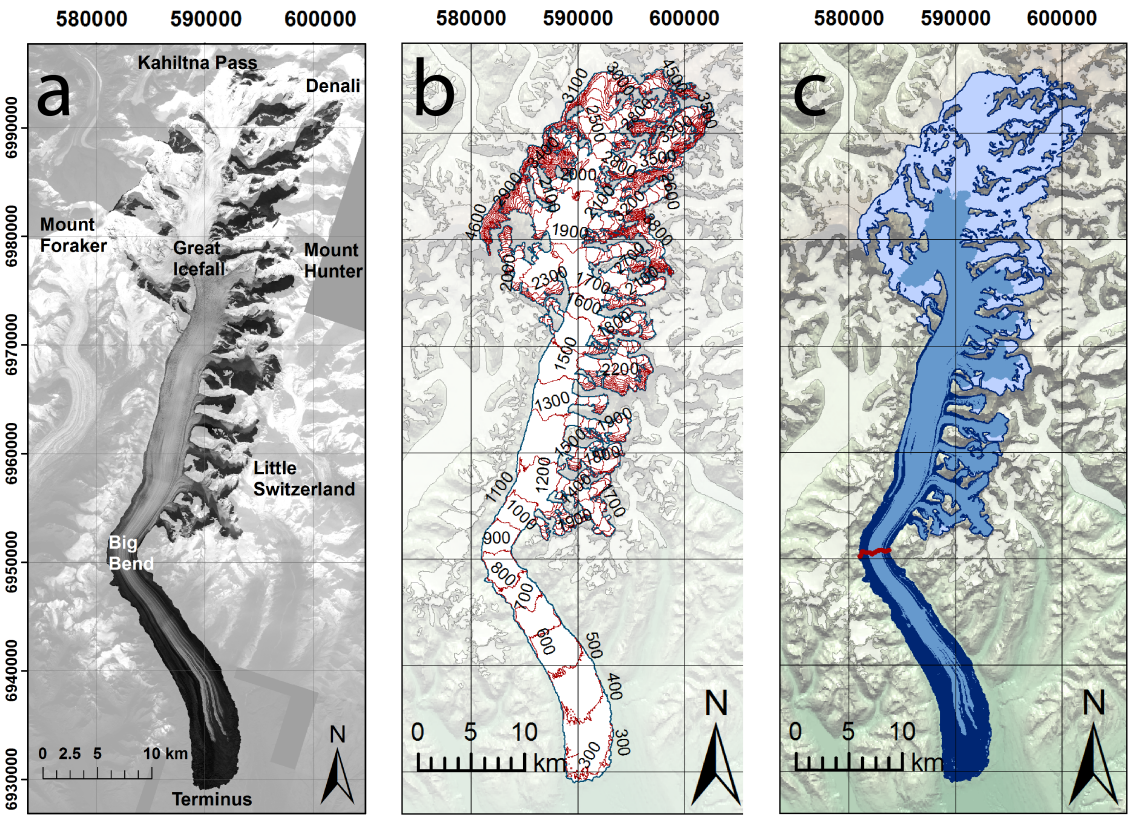

Figure 1.2. Maps of relevant features and zones on and near the Kahiltna Glacier. a) Geographical areas of interest and high peaks surrounding the Kahiltna Glacier, displayed on a backdrop of orthoimagery collected by the Alaska Statewide Mapping Initiative. b) Contour map, with elevations calculated from a 2011 Interferometric Synthetic Aperture Radar Digital Elevation Model. c) Debris map, with debris-covered ice shown in dark blue, as identified from Landsat 5/7 ETM+ imagery using a band ratioing technique (pers. comm. S. Herreid, 2011). Estimated firn areas are shown in light blue, as derived from aerial photographs and long-term field observations by the NPS. All maps are in UTM zone 5V coordinates.

significant lateral Little Ice Age moraines (Burrows and Adema, 2011). All summer melt leaves the glacier via 2 to 4 main channels that coalesce downstream to form the Kahiltna River, which ultimately drains into the Gulf of Alaska.

1.1.2 Background on National Park Service research

Mass balance monitoring in the Central Alaska Range was pioneered in the late 1990s by Lawrence Mayo (Mayo, 2001). In his guide to monitoring glaciers using the index method, Mayo describes the selection criteria (namely large size, non-surge-type behavior, and climate regime) used to establish long-term monitoring sites on both the Kahiltna Glacier on the south side of the range, and the Traleika tributary to the Muldrow Glacier on the north side. At each of these, based on Mayo's recommended minimum observations, bi-annual mass balance measurements have been collected since 1991 at a single location near each glacier's long-term average ELA. The ELA was established by installing two mass balance stakes at different elevations (1540 m and 1930 m) between 1992 to 1995, in order to determine an average annual balance gradient and, in turn, the associated average zero-balance elevation. Observations were then reduced to the single long-term stake located near the average ELA (1925 m), following the theory that mass balance at this elevation should be zero in steady-state or should otherwise fluctuate in response to positive or negative balance years, ultimately serving as a good indication of the total mass balance of the glacier (Ohmura and others, 1992).

The NPS index sites represent among the longest continuous records of glacier mass balance measurements available for any Alaskan glaciers. Long-term records like these are of critical importance to the success of mass balance modeling of past and future changes, and for ground-truthing of remote sensing methods. To date, little analysis has been carried out on the summer, winter and annual mass balance measurements reported by Burrows and Adema (2011) (Fig. 1.3). Moreover, although additional monitoring has also been carried out in the park using repeat photography and terminus mapping, revealing patterns of thinning and retreat, these visual changes have not been quantified.

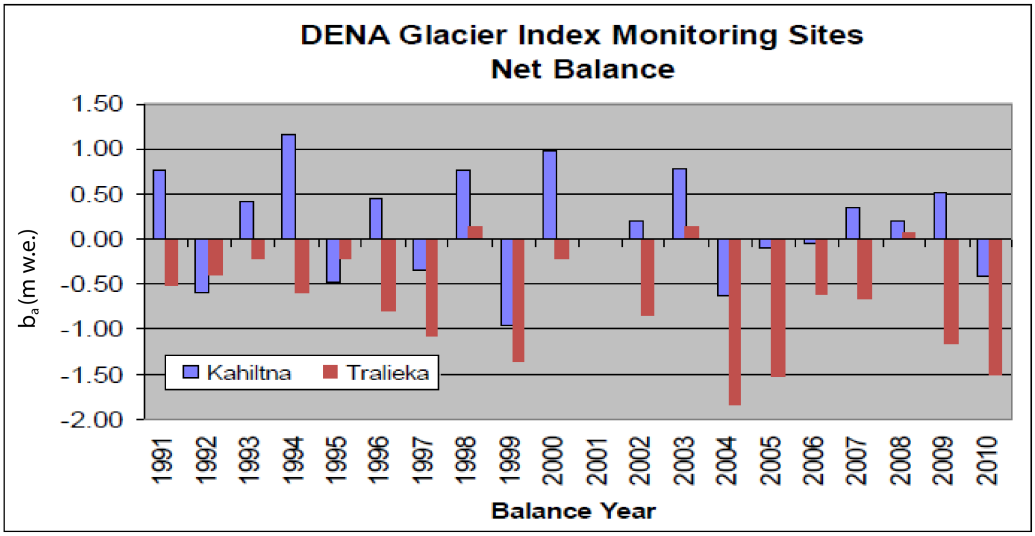

Figure 1.3. Annual balance measurements b_a at the NPS index site locations on Kahiltna and Traleika Glaciers (Figure reproduced from Burrows and Adema, 2011). The NPS typically carries out twice-annual measurements at each of these sites, but does not extrapolate these point observations to determine glacier-wide balances.

Chapter 2

2.1 Data

2.1.1 Data for model

Model simulations are divided into two different time periods. In 2010 and 2011, we collected field measurements of air temperature and mass balance, to serve as input and calibration data. We calibrate our melt model using our 2011 mass balance measurements because they are of better quality, and then validate our parameter choices using our 2010 data. Once tuned, we then apply the model retroactively to 1991 using supplementary temperature and precipitation data. This time period allows us to compare our model results to both the measurement record from the NPS (Fig. 1.3) as well as to estimates derived from airborne altimetry. Mass balance and air temperature data used for the model are described below, first for the 2010 and 2011 calibration and validation years, and then for the 1991 to 2009 hindcasting period.

2.1.1.1 Mass balance

Conventional mass balance observations were carried out on the Kahiltna Glacier in 2010 and 2011 (Fig. 2.1), following standard methods (Østrem and Brugman, 1991; Mayo, 2001; Cogley and others, 2011). Snow depths were recorded in late spring by taking an average of three to five depth measurements using a graduated avalanche probe at 71 locations between 792 and 1385 m in 2010, and 83 locations between 802 m and 1385 m in 2011, along the glacier centerline (Fig. A.2; Tables A.5 and A.6). We covered an elevation range that was limited by safe ski travel and that represents ∼25% of the total glacier area. Snow densities were measured vertically through the snowpack using a 0.5 L volume sampler and spring scale, at three snow pits in 2010 (808 m, 1099 m and 1235 m) and two in 2011 (994 m and 1212 m; Fig. A.2; Tables A.3 and A.4). Winter balance was then calculated by applying each year's average depth-density function determined from the snow pits to the measured snow depths at each site, based on the assumption that the measurement date captured the winter snow water equivalent maximum (i.e. that any early-season meltwater had percolated and refrozen within the year's snowpack).

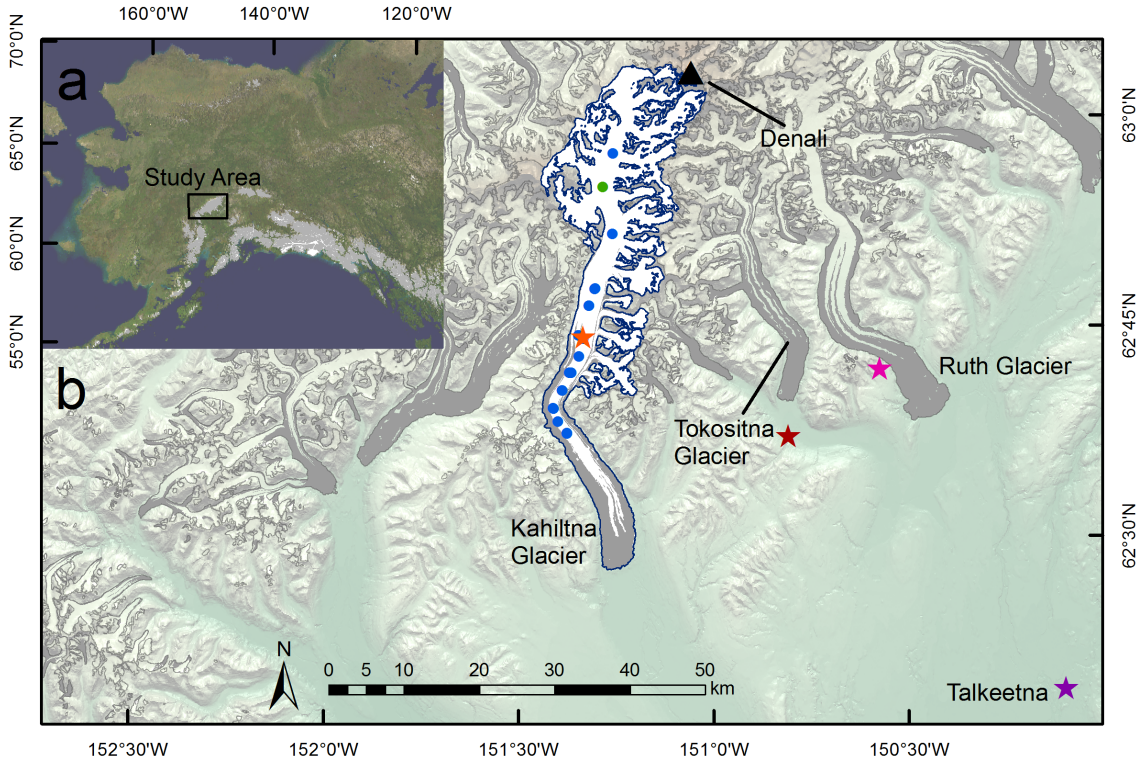

Figure 2.1. Location of the Central Alaska Range and Kahiltna Glacier, and nearby weather stations. a) Location of the Central Alaska Range within Interior Alaska, with glacierized terrain shown in light grey. b) Location of the Kahiltna Glacier, outlined in blue, within the debris-covered glaciers of the Central Alaska Range. 2010 and 2011 campaign mass balance stakes are shown in blue, spanning an elevation range of 791 m to 2004 m, and the long-term NPS stake at 1925 m used for model hindcasting is shown in green. Weather stations are indicated by stars; orange indicates the location of the automated weather station we installed for a one-year period, pink shows a site adjacent to Ruth Glacier maintained by NPS, red designates a Snowpack Telemetry site in the Tokositna valley, and purple indicates a long-term airport station in Talkeetna.

Ablation stakes were installed along the centerline at 9 elevations between 808 m and 1409 m in 2010, and 11 elevations between 791 m and 2004 m in 2011 (Figs. 2.1 and A.1; Tables A.1 and A.2). Stakes were either aluminum tubing, or PVC pipes strung together in a fashion similar to collapsible tent poles. Snow and ice melt were converted to water equivalent units using the average snow depth-density function, and an assumed ice density of 900 kg/m^3, respectively. The NPS index site stake is located at 1925 m near the estimated ELA of the glacier (Burrows and Adema, 2011) (Fig. 2.1).

2.1.1.2 Initial 2010 and 2011 snow cover

To characterize glacier-wide winter balance for use in the model for each of 2010 and 2011, we require a supplemental product to help guide the extrapolation of our in-situ point measurements to the full glacier extent. Because our ground measurements show high spatial variability over the small elevation range spanned, and reveal no strong trend with elevation (Tables A.5 and A.6), extrapolation is not robust using in-situ data alone. We therefore integrate our measurements with 2 x 2 km grids of monthly average precipitation from 1971 to 2000 from the Parameter-elevation Regression on Independent Slopes Model (PRISM) climate product (Daly and others, 1994, 2002). PRISM uses point climate data from weather stations and incorporates a digital elevation model to produce continuous grids of mean monthly precipitation. We choose PRISM because it has a high spatial resolution, takes orographic effects into account, and has been found to have the best spatial coverage of Alaska mean monthly precipitation and surface temperature, based on validation with independent in situ data (Simpson and others, 2005).

We sum together all monthly precipitation grids where the associated monthly temperature at a particular elevation is $T_{air} < 0°C$ (October to April inclusive, with some elevations also receiving snowfall in September and May). This yields a 2 x 2 km winter balance grid that we sample along the glacier centerline over the full elevation range (Fig. 2.2). We smoothly interpolate this using a locally weighted linear regression to yield an elevation-dependent profile of mean winter balance (Fig. 2.3). Until $\sim$2000 m, this profile is characterized by nearly linear precipitation increase with elevation, agreeing with ground-penetrating radar observations along several other Alaska glacier centerlines (pers. comm. A. Gusmeroli, 2013). Above 2000 m (for the uppermost 35% of the glacier area), orographic

effects simulated by the PRISM model become important, resulting in a negative precipitation gradient at higher elevations.

We next shift this mean winter balance distribution based on our annual in-situ winter balance data for 2010 and 2011 (Tables A.3, A.4, A.5 and A.6). Because point measurements are so variable over the small elevation range spanned, we take the average winter balance measured and the associated elevation as a tie point for shifting the profile for each of 2010 and 2011 (Fig. 2.3). Finally, we spatially distribute these annual profiles of winter balance with elevation to the full glacier using a 25 m Interferometric Synthetic Aperture Radar (IFSAR) DEM constructed in July 2011 (described in greater detail in Sec. 2.1.2.2) (Gesch and others, 2002; Gesch, 2007), to obtain the 2010 and 2011 winter snow cover grids needed for model input. As a last step, we overwrite the values at the grid cells corresponding to our stake locations with our actual measured winter balances at those sites. This ensures that model calibrations, which compare measured to modeled melt at those exact stake locations, are carried out using the best available data for end-of-winter conditions at those points.

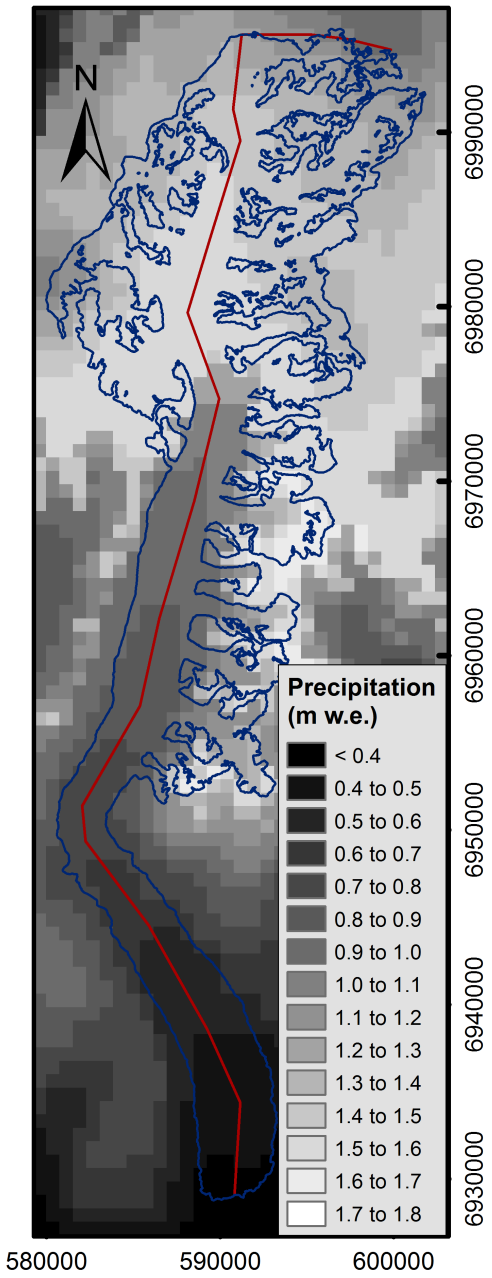

Figure 2.2. Centerline sampling technique for generating winter precipitation input from PRISM climate product. Total winter snowfall estimated as the sum of all precipitation at a given elevation for months with corresponding average air T < 0°C (October to April inclusive, with some elevations also receiving snowfall in September and May). Precipitation data are 30-year (1971 to 2000) means from the PRISM dataset (Daly and others, 1994, 2002). Values are extracted along a centerline (red).

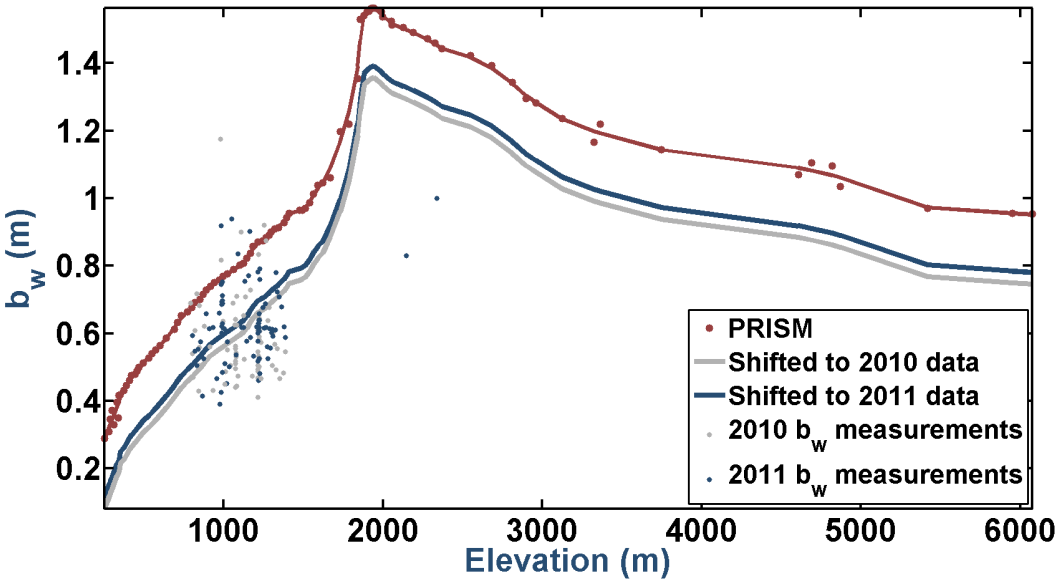

Figure 2.3. Elevation-dependent profile of winter balance derived from PRISM climate product. Red data points show sampled values from the summed winter PRISM grids, smoothed and interpolated to yield an elevation-dependent winter balance profile. Grey and blue profiles are determined for 2010 and 2011 by shifting to the mean ground measurement and associated elevation for each year. Grey and blue point data shows all winter balance measurements collected in 2010 and 2011, demonstrating the high degree of variability seen over the sampled elevation range.

2.1.1.3 Precipitation

During the winter of 2010/2011, we installed a MaxBotix MB7060 sonic ranger at 1214 m elevation to estimate snow accumulation. Unfortunately, though the timing of accumulation events is clear within the record, we experienced problems with sensor drift, as determined by comparing the recorded snow depth to multiple measurements of depth by snow probe at the end of the winter season. This produced sonic ranger records that are unusable for estimating accumulation magnitudes. We therefore compare the record to available precipitation datasets to determine the magnitudes of snowfall events needed for model input. We compare to: a) a National Oceanic and Atmospheric Administration (NOAA) airport weather station in Talkeetna, southeast of the Central Alaska Range; b) a Natural Resources Conservation Service (NRCS) Snowpack Telemetry (SNOTEL) station located ~25 km away and at approximately the same elevation as the glacier terminus;

and c) an upper-air reanalysis climate data product from the National Centers for Environmental Prediction and National Center for Atmospheric Research (NCEP-NCAR), at a node located ∼60 km from the glacier. All options are listed in Table 2.1 and shown in Fig. 2.1. Note that we use the NCEP-NCAR product 'NOAA NCEP-NCAR CDAS-1 mc8110,' a daily product based on a 1981 to 2010 climatology, available at a spatial resolution of ∼2.5° x 2.5° (Kalnay and others, 1996). The SNOTEL station, which records snowpack water equivalent by means of a snow pillow and which is the nearest to the Kahiltna Glacier geographically, is found to have the best visual correlation to our on-glacier sonic ranger snowfall event timing (Fig. 2.4). We therefore use this SNOTEL data for our 2010 to 2011 model simulations, but as the station was not installed at an early enough date, we turn to NCEP-NCAR records for the hindcasting period (Fig. 2.5).

To scale precipitation event records to the Kahiltna Glacier, we compare our 2010 and 2011 winter balance measurements at 1409 m (the elevation of our air temperature model input, described in Sec. 2.1.1.4), to corresponding cumulative observations from the SNOTEL and NCEP-NCAR sources at the same time as our in-situ observations. We obtain the average scaling factor for each two-year comparison, and respectively apply these to the SNOTEL record for 2010 to 2011 and retroactively to the NCEP-NCAR record for 1991 to 2009.

Next, to distribute these precipitation events to the full glacier extent, we use the elevation-dependent profile of mean winter balance we derived by summing together monthly precipitation means from PRISM (Sec. 2.1.1.3). We normalize the profile to the elevation of our AWS at 1409 m, and determine the slope of each portion of the normalized profile above and below 2000 m. These linear precipitation gradients are then applied to distribute any single precipitation event from the point location at 1409 m to grid cells at all elevations of the glacier, using the 25 m IFSAR DEM described in Sec. 2.1.2.2 (Gesch and others, 2002; Gesch, 2007).

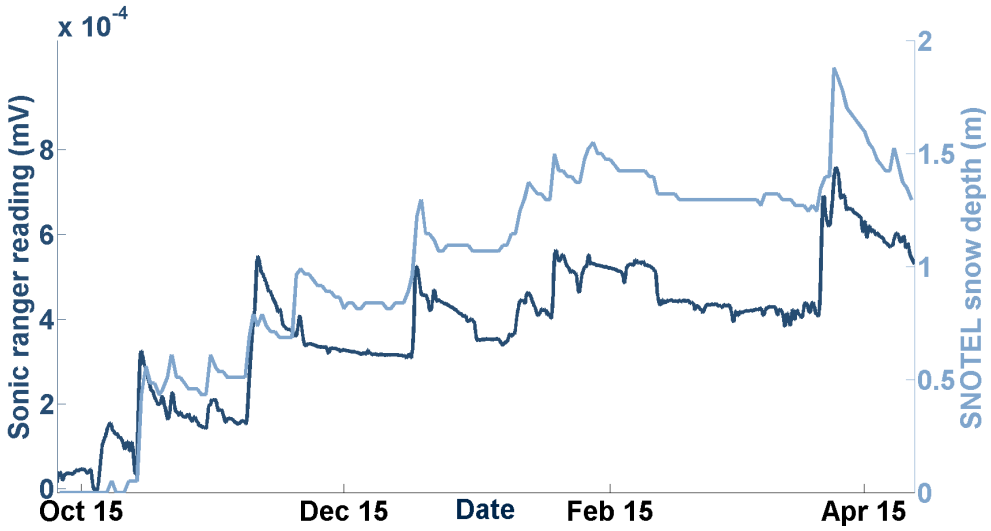

Figure 2.4. Comparison of precipitation event timing from our in-situ sonic ranger to a snowfall record from the nearby SNOTEL station in Tokositna valley. We use this hourly record to drive our 2010 to 2011 model simulations.

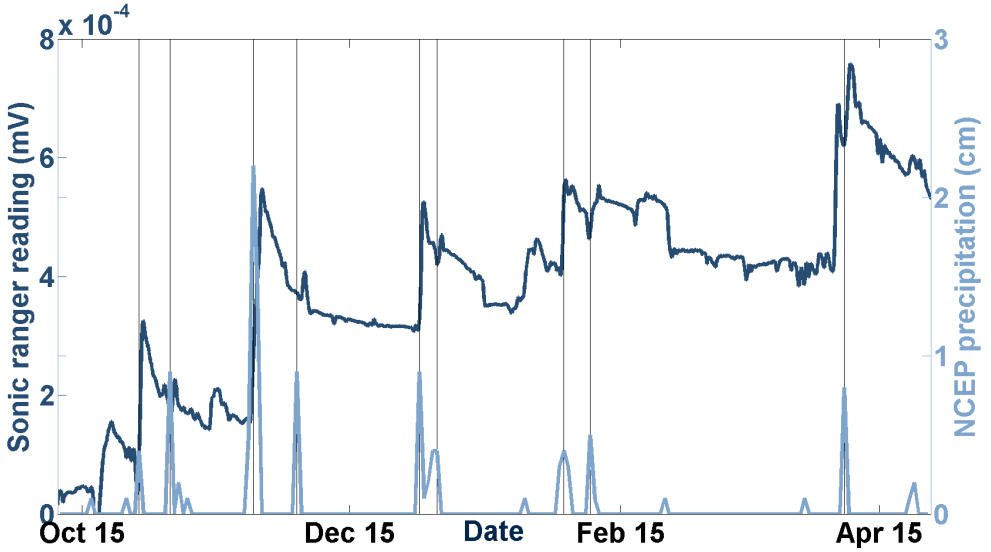

Figure 2.5. Comparison of precipitation event timing from our in-situ sonic ranger to NCEP-NCAR reanalysis data. We use this daily record of precipitation to drive our 1991 to 2009 model hindcasting simulations.

Finally, in order to assess our method for characterizing the timing and magnitude of snowfall events on the glacier, which can be particularly challenging with summer air temperatures that are often near $0^{\circ}C$, we visually compare Landsat 5/7 ETM+ images to the surface type evolution from snow-covered to bare ice during preliminary model simulations. Though only two clear-sky images are available for the Kahiltna Glacier for each of the 2010 and 2011 melt seasons, we find that the modeled evolution of the snowline is slower than seen in the satellite images. We therefore elect to turn off precipitation events during a two-month summer period (equivalent to precipitation falling as rain instead of snow), based on the time stamps of the available imagery. This yields a better match of modeled surface type to the optical satellite imagery.

2.1.1.4 Air temperature

Onset HOBO U23 Pro v2 air temperature sensors recorded 10-min measurements at five elevations on the glacier between 808 m and 1409 m in summer 2010, and 791 m and 1396 m in summer 2011. Accuracy of the sensors is reported as $\pm 0.21^{\circ}$C for temperatures above 0°C. These were installed on floating PVC stands fitted around the existing aluminum mass balance stakes and designed to remain at a constant height above the glacier surface (see Sec. A.2) (Young and others, 2011). Unfortunately, the original stand design failed to slide down the stake at some sites, lodging the sensors at varying heights above the surface. We therefore linearly interpolate the sensor sampling height between visit dates. Though it is well-known that air temperatures follow a logarithmic profile above a glacier surface (Oerlemans, 2010), we lack sufficient in-situ data to fully characterize this profile for the Kahiltna Glacier. Instead, we adjust the temperature records to a standard 2 m sampling height at each time stamp using an empirically-derived vertical profile determined from the land-terminating Morteratschgletscher in Switzerland (Oerlemans, 2000), as this is the only study to fully characterize this profile based on actual ground observations (see Sec. A.2.1 for correction details). Applied to our temperature records, this yields an average change of 0.18°C in 2010 and -0.12°C in 2011.

On-glacier temperatures were also measured with an Onset 12-bit Smart Sensor installed at 1214 m between Sept. 2010 to April 2011. This sensor was affixed to steel tubing drilled vertically into the ice surface. Data collected prior to burial by snow is used to fill in gaps

in the HOBO record in late summer 2010.

For our 2010 and 2011 simulations, we drive the model with our highest-elevation summer sensor (1409 m) and calibrate the modeled mass balance against our stake measurements. After this, since our field campaigns did not capture the full summer melt period, we fill early-spring and late-summer gaps in our sensor records using data from the nearest available source: a Remote Automated Weather Station (RAWS) near the neighboring Ruth Glacier (Table 2.1). We correct for elevation differences between our sensors and the bedrock station using the standard environmental lapse rate (-6.0°C km^{-1}). Piecing together these records ensures that we capture the full stratigraphic balance year. Temperatures are hourly-averaged.

Lapse rates are determined for each hourly time step by linear regression between all five sensors when data are available and, for the early-spring and late-fall melt periods outside of our measurement window, by constant average lapse rates from the respective first and last months of measurements.

We analyze the suitability of air temperature data for the 1991 to 2009 hindcasting period by comparing our summer 2010 and 2011 on-glacier measurements to nearby weather station records and reanalysis products (Fig. 2.1; Table 2.1). NCEP-NCAR (Kalnay and others, 1996) correlates best (R^2 = 0.75), and is therefore our choice for driving the hindcast model simulations. Note that in all cases, we compare the record to each of our five on-glacier HOBO temperature sensors, and find the best correlation at our highest-elevation sensor (1409 m).

NCEP-NCAR temperature fields at the 850-hPa isobar level correlate better to our in-situ measurements than those from the 700-hPa or 925-hPa isobar levels, or from interpolation between isobar geopotential heights to our on-glacier temperature sensor elevation. The 850-hPa level corresponds to a geopotential height ranging between ∼1000 m to 1500 m. The strong correlation with this isobar agrees with previous findings (Rasmussen and Conway, 2004), as this upper-air level shows temporal variability that often matches the processes of mass balance – ablation and accumulation – better than more localized climate drivers. We determine a linear relationship between our on-glacier temperatures at 1409 m and NCEP-NCAR at 850 hPa, and invert this relationship to adjust the long-term NCEP-NCAR record to on-glacier conditions. The resulting temperature time series has

Table 2.1. Air temperature dataset options for driving the 1991 to 2009 model hindcasting period. Each hourly record is compared to on-glacier measurements to determine correlation, and the dataset with the highest correlation (NCEP-NCAR) is selected for use as input data.

DataSet	Type	Location	Latitude (° N)	Longitude (° W)	Distance from glacier (km)	R^2
NOAA	AWS	Talkeetna	62.32	150.09	60	0.70
SNOTEL	AWS	Tokositna	62.63	150.78	25	0.61
NCEP-NCAR	upper-air	N/A	62.50	152.50	60	0.75
RAWS	AWS	Ruth valley	62.71	151.53	40	0.72

a signal amplitude that is dampened relative to the NCEP-NCAR record, as would be expected for air temperatures above a snow/ice surface fixed at 0°C, rather than bare ground or bedrock (Oerlemans, 2010).

Finally, for the hindcasting period, we use daily-averaged lapse rates from the 2011 summer field season (Fig. 2.14), given better quality temperature data from that year (requiring less correction to the logarithmic profile described in 2.1.1.4 and A.2.1. Gaps outside of the melt period are filled with the environmental lapse rate (-6.0°C km^{-1}).

2.1.1.5 Glacier outline

We use a manually-delineated outline for the Kahiltna Glacier based on a mosaic of Landsat 5/7 ETM+ images from the mid-2000s, available from the Randolph Glacier Inventory v3.2 (Pfeffer and others, In Press).

2.1.2 Remote sensing data

2.1.2.1 Airborne laser altimetry

Glacier surface height changes are measured via repeat airborne laser altimetry, a technique carried out by the University of Alaska Fairbanks laser altimetry group. Mounted in a small airplane, the system is composed of a high-accuracy Global Positioning System (GPS) receiver, a laser rangefinder, and an inertial navigation system. The GPS records the position of the plane as it flies down a glacier centerline, the laser continuously measures the distance between the plane and the ice surface, and the inertial navigation system measures the laser's pointing direction. From these, centerline surface elevation profiles are created.

Two types of laser systems have been employed for this task: (1) a nadir fixed laser that collects a single profile of measurements along the flight path (profiler), and (2) a scanning laser that sweeps up to 30° off-nadir, yielding a swath of measurements (scanner). The profiler served as the pioneering laser altimetry system described in earlier publications (Echelmeyer and others, 1996; Arendt and others, 2002; Johnson and others, 2013), with an along-track laser shot spacing of 1.2 m. It was replaced by the laser scanner – currently a Riegl LMS-Q240i – in 2009. The scanner has a sampling rate of 10,000 Hz and, when positioned at an optimum aircraft elevation of 500 m above the glacier surface, produces an average swath of 500 m and return spacing of 1 m x 1 m. In both systems, the laser has a wavelength of 905 nm, and a shot footprint of 20 cm.

Glacier surface elevations are derived by combining laser return data with airplane positioning and attitude data from the onboard Global Positioning System-Inertial Navigation System (GPS-INS). Each return point is referenced in ITRF00, and coordinates are projected to WGS84 UTM Zone 5N. The aircraft position is processed from both L1/L2 data, using the Gamit-Globk differential phase kinematic positioning program 'Track' (Chen, 1998; King, 2009). Data from all time periods and both laser systems have been processed similarly to ensure direct comparisons can be made between all profiles. The Kahiltna Glacier was surveyed by laser profiler on July 31, 1994 and May 18, 2008, and by laser scanner on May 22, 2010, enabling three different mass balance estimates for 1994 to 2008, 1994 to 2010 and 2008 to 2010. A fourth time period is also included in our analysis from an earlier

comparison of the 1994 flight line to an extracted centerline from a historical 1951 DEM (Arendt and others (2002); DEM is described in greater detail in Sec. 2.1.2.2). To date, a comparison of the 1951 map date to 2010 flight profiles has not been carried out, but we derive an estimate for this time period by combining our estimates from 1951 to 1994 and 1994 to 2010 using a weighted mean.

2.1.2.2 Digital elevation models

To represent the glacier's modern day topography, we use an Interferometric Synthetic Aperture Radar (IFSAR) digital elevation model (DEM), based on imagery acquired in July 2011 as part of the Alaska Statewide Mapping Initiative (Gesch and others, 2002; Gesch, 2007). The X-band (3 cm wavelength) radar used for this purpose has minimal penetration depth over glacier ice, but up to 5 to 10 m over dry firn. The DEM has horizontal and vertical datum of NAD83 and NAVD88, 5 m postings, and approximate RMS elevation errors of 1.57 m in areas with slopes <10% (66% of the total glacier area) and 5.12 m in areas with slopes of 10 to 20% (16% of the glacier area) (Mantey, 2012). Errors beyond this range are currently unquantified; we therefore also classify error for slopes >20% as 5.12 m (18% of the glacier area).

To fill in a small region of missing IFSAR data in the northernmost region of the glacier, and for DEM differencing, we also employ a historical US Geological Survey DEM from the National Elevation Dataset (NED) (Gesch and others, 2002; Gesch, 2007). The NED DEM for the Kahiltna Glacier was derived by digitizing contour maps created from aerial photographs collected between 1951 and 1954. The exact date of these maps is not well known due to multiple aerial photo campaigns and limited metadata describing which images were used to create individual map sheets. We therefore conservatively define the NED map date as 1951, following Arendt and others (2002). The NED has a horizontal and vertical datum of NAD27 and NGVD29, and a grid spacing of $\sim$45 m. Unfortunately, the product is known to have inaccuracies due to poor contrast at high elevation accumulation zones, where featureless snow cover is a challenge for photogrammetric mapping (Arendt and others, 2002; Larsen and others, 2007). Nominal map elevation errors are defined for the ablation area as one-half a contour, or $\pm$15 m, and for the accumulation area as one full contour, or $\pm$30 m. These errors are discussed in further detail in Sec. 2.3.2.2.

2.1.2.3 Satellite gravimetry

Mass variations of glaciers and ice sheets are, in some regions, of sufficient magnitude to significantly alter local gravity fields. Tracking of these temporal gravity variations has been accomplished through precise measurement of changes in range between two low Earth co-orbiting satellites (Luthcke and others, 2013). These range-rate observations are controlled primarily by gravitational potential differences between each satellite, which at any given location is the sum of contributions from Earth and ocean tides, and mass changes due to oceans, atmosphere, and land ice (Luthcke and others, 2013). For studies of land ice variations, forward-models and observations of non-glacier signals are used to isolate the glacier mass balance signal.

Here we examine satellite gravimetry data from NASA's Gravity Recovery and Climate Experiment (GRACE) tandem satellites. GRACE has been applied extensively to glaciers of the Gulf of Alaska region (Tamisiea and others, 2005; Chen and others, 2006; Luthcke and others, 2008; Wu and others, 2010; Pritchard and others, 2010; Jacob and others, 2012; Sasgen and others, 2012; Luthcke and others, 2013), due to their relatively large seasonal and long-term rates of mass change. The range of publications for Gulf of Alaska glaciers reflects variations in Level 1 GRACE products from different processing centers, as well as differences in methods for filtering and correcting the observations to isolate glacier mass balances from other sources of mass change. Here we use NASA's Goddard Space Flight Center high resolution mass concentration (hereafter, mascon) GRACE solution. This solution provides mass change estimates at 10-day temporal and 1° x 1° (approximately 25,000 km^2) resolution (Arendt and others, 2013). We choose this dataset because it is one of few that explicitly corrects for local mass increases associated with post-Little Ice Age disintegration of the Glacier Bay icefield (Larsen and others, 2005). It also uses a processing method that enables examination of mass changes at each 1° x 1° mascon location.

2.2 Methods

2.2.1 Model

We carry out model simulations over two separate periods: first, we calibrate and validate the model for 2010 and 2011 using our field measurements, and then use the tuned model

to hindcast 1991 to 2009. The combined results spanning 1991 to 2011 are then compared to mass balance estimates from three remote sensing techniques.

2.2.1.1 Model description and application

We implement a fully distributed degree-day model to determine mass balance at every grid cell on the glacier (Hock, 1999). The model uses near-surface air temperature as a proxy for the dominant energetic processes of ablation, including radiation and turbulent heat fluxes. Shading is taken into account using solar geometry and surrounding topography, by implementing an algorithm that determines the mean potential direct solar radiation for each grid cell. Melt at every time step is ultimately determined by:

$$M = (F_m + a_{snow/ice} * I) * T^+ \tag{2.1}$$

where M is melt in water equivalent units, T^+ is the positive air temperature in °C, and I is the potential direct solar radiation calculated at every time step. F_m is the melt factor in mm day^{-1}K^{-1}, and a_{snow} and a_{ice} are the radiation factors for snow and ice in mm m^{2}W^{-1}day^{-1}K^{-1}. Together, these three variables form our suite of tuning parameters.

We also incorporate debris cover, as derived from a band ratioing technique applied to Landsat 5/7 scenes using bands 3 and 5 (pers. comm. S. Herreid, 2011). Numerous studies have derived empirical relationships that relate debris layer thickness to the amount by which melt is enhanced or suppressed (Østrem, 1959; Mattson and others, 1993; Kayastha and others, 2000). These 'Østrem curves' suggest that at a thickness of ∼2 to 4 cm, debris has a negligible effect on melt rates as compared to bare ice. Five ground observations on the Kahiltna Glacier indicate an average depth of 3 cm, with a range between 1 to 5 cm, as sampled on several medial moraines in different locations. From this information, we assign the same melt factor to debris-covered ice as to bare ice. However, our measurement sample size is small, so we consider our choice for this factor to be a source of uncertainty. We therefore carry out sensitivity tests to assess the importance of correctly characterizing this melt-modifying parameter.

Finally, we choose a precipitation threshold of 1.5°C (pers. comm. A. Rasmussen, 2011), meaning that precipitation falls as snow for any temperature below this value. The model time steps for the 2010 to 2011 and 1991 to 2009 periods are respectively hourly and daily.

2.2.1.2 Model calibration

To calibrate the model, we compare model-generated mass balance to measured mass balance at the ablation stake locations (Tables A.1 and A.2). We carry out the 2010 and 2011 model simulations independently, optimizing our parameter set to reproduce the mass balance observed at our stakes between measurement dates. We use 2011 as our calibration year, based on several factors: a) the annual balance gradient from our observations is a better match to the long-term gradient measured by the NPS (0.0032 m w.e. per meter elevation; see Sec. 1.1.2) (Burrows and Adema, 2011); b) our input air temperature data were sampled at more consistent heights above the ice surface, requiring less correction to the standard 2 m sampling height than our 2010 data; and c) 2010 was widely observed as a year with unusually small mass losses in Alaska (this is especially visible in the GRACE record). We therefore focus our calibration efforts on our 2011 measurements, considering this data to be more robust and representative of a typical mass loss year. We then validate our optimized 2011 parameter set against 2010. For each year, we use a batch routine to perform 260 model simulations, initially covering a broad range of parameter values (Fig. 2.6), then focus more narrowly for fine-tuning (Fig. 2.7). As many model simulations yield similar R^2 values, we prioritize the minimization of root mean square error (RMSE) when calibrating. We select the five best 2011 parameter sets (Table 2.2), as RMSE values associated with these fall within 5% of one another. We then validate against our 2010 results using the five best 2010 parameter sets. Annual balances for each year are taken as the mean of all five simulations.

When we apply 2011 parameter choices to our 2010 data, though the calculated R^2 values between modeled and measured point mass balances do not change, RMSE increases substantially. Unfortunately, balances calculated are also twice as negative as the values we calculate using our 2010 parameter sets. This difficulty in reproducing our 2010 results using 2011 parameters on 2010 data demonstrates the high sensitivity of our model simulations to our choice of parameters, given that the same climate input data can yield substantially different annual balances using different parameters.

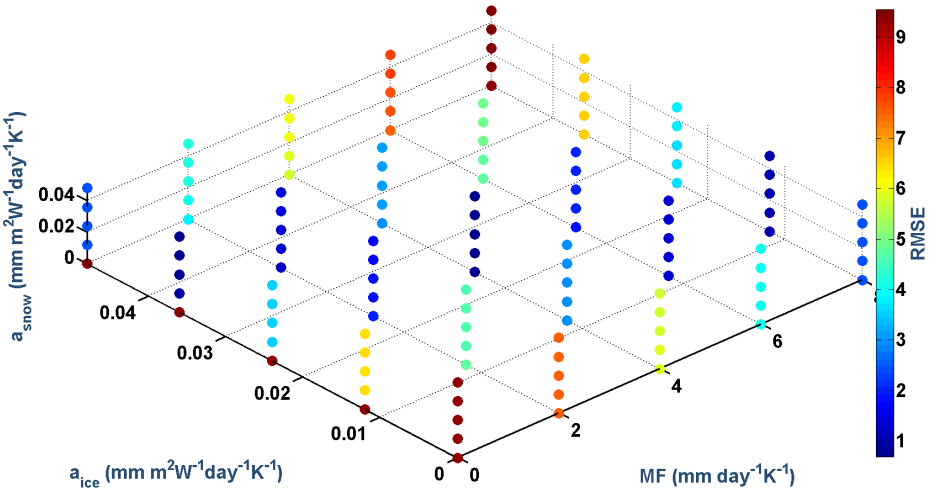

Figure 2.6. Parameter space for initial batch of 2011 calibration year model simulations. RMSE between modeled and measured melt at stake locations is shown for the initial broad range of parameter values tested.

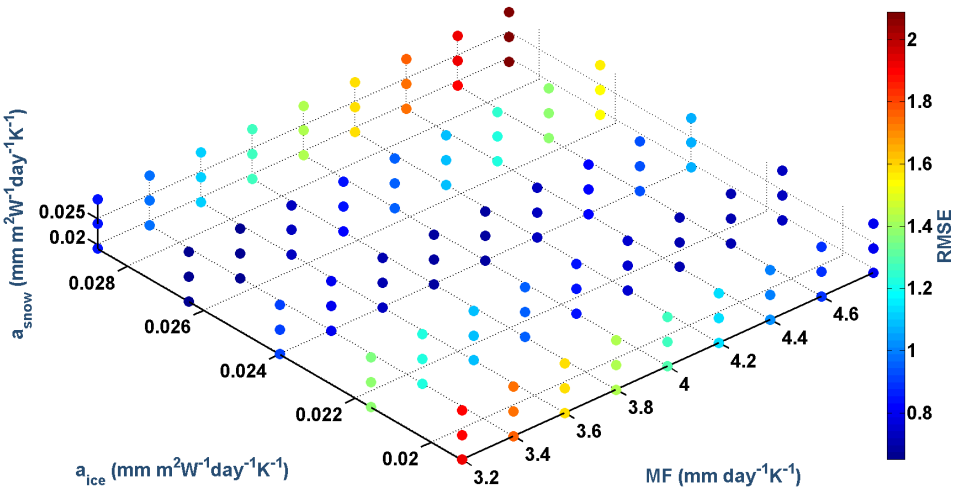

Figure 2.7. Parameter space for fine-tuning 2011 calibration year model simulations. RMSE between modeled and measured melt at stake locations is shown for the narrowly-focused range of parameter values tested.

Table 2.2. Best parameter sets for 2010 and 2011 model simulations. The five best sets are selected for each year, prioritizing the minimization of RMSE between modeled and measured mass balance at stake locations.

Year	MF (mm day^{-1}K^{-1})	a_{ice} (mm m^{2}W^{-1}day^{-1}K^{-1})	a_{snow} (mm m^{2}W^{-1}day^{-1}K^{-1})	RMSE m w.e.	R^2
2010	3.4	0.6	0.5	0.62	0.83
	4.2	0.5	0.3	0.63	0.83
	4.8	0.4	0.3	0.63	0.83
	3.4	0.6	0.3	0.63	0.83
	3.6	0.6	0.3	0.63	0.83
2011	3.2	1.1	1.0	0.65	0.91
	3.2	1.1	0.8	0.66	0.91
	3.4	1.1	1.0	0.67	0.91
	3.4	1.1	0.8	0.67	0.91
	3.8	1.0	0.8	0.68	0.91

2.2.1.3 Model hindcasting

Using the five optimized parameter sets determined from the 2011 model simulations, we carry out simulations for 1991 to 2009 using air temperature and precipitation from the NCEP-NCAR reanalysis product, scaled to on-glacier conditions. Forcing data choices and adjustments are described in Sec. 2.1.1. To assess model performance, we compare modeled balances to the 20-year observation record at the NPS index site (Burrows and Adema, 2011), and to bulk mass change estimates from laser altimetry for the overlapping time period. We also compare to independent estimates from DEM differencing and satellite gravimetry.

2.2.2 Remote sensing techniques

2.2.2.1 Airborne laser altimetry

Analysis of airborne laser altimetry data is carried out at the University of Alaska Fairbanks, according to published methods (Arendt and others, 2008; Johnson and others, 2013). To obtain glacier-wide mass balance estimates, surface height changes are derived by differencing successive elevation profiles, and dividing by the time elapsed between profiles to arrive at elevation change rates. These are extrapolated from the centerline flight paths to the full surface area of the glacier using elevation bins derived from the 2011 IFSAR DEM, to yield volume change estimates (Johnson and others, 2013). Next, volume changes are converted to water equivalent units using a density of 850 $\pm$60 kg m^{-3} (Huss, 2013). This value, which is lower than the conventional 900 kg m^{-3} often used to convert geodetic changes to volume loss based on Sorge's Law (Bader, 1954), is explained by the removal of low-density firn layers and subsequent changes in the firn density profile with negative balance. Since the Kahiltna Glacier is known to have a large firn area(Gusmeroli and others, 2013), resulting from recent mass losses that have exposed firn over a large and flat portion of the main glacier trunk, we believe this value is an appropriate choice of conversion factor for this glacier. Finally, mass changes are integrated over the full glacier extent.

The Kahiltna Glacier has been surveyed by laser altimetry three times, on July 31, 1994, May 18, 2008, May 22, 2010. A seasonal correction is required for estimates derived using the 1994 data, given that it was acquired at a different time of year (summer versus spring). To quantify this correction, we add a glacier-wide winter balance derived from monthly precipitation means from the PRISM dataset (Sec. 2.1.1.2). This yields a mean change of 1.11 m yr^{-1}. Adding this winter balance simulates acquisition in spring 1995, to match the spring acquisition times for 2008 and 2010. We then divide by one year less to determine the average annual balance.

2.2.2.2 DEM differencing

To gauge the success of the extrapolation techniques employed in laser altimetry, the validity of which has been questioned in Berthier and others (2010), we also derive mass change estimates from DEM differencing. Both of these techniques measure glacier surface height changes, such that we can directly compare the spatial patterns of height changes and the glacier-wide mass balance estimates derived from each.

To determine glacier-wide surface height changes, a 1951 US Geological Survey DEM from the National Elevation Dataset (NED) is compared to a 2011 Interferometric Synthetic Aperture Radar (IFSAR) DEM from the statewide Alaska mapping initiative (Gesch and others, 2002; Gesch, 2007). Note that at the time of analysis, the IFSAR DEM did not cover the full extent of the Kahiltna Glacier, such that a portion of the 1951 NED was stitched into the northernmost regions of the glacier. Also, because of a difference in vertical datum (NGVD29 for the NED, versus NADV88 for the IFSAR), a 2 m correction is systematically applied to raise the NED. Because NGVD29 is not defined in Alaska, no single program exists to transform between the two systems. The correction is therefore determined as the average offset between benchmark measurements (Arendt and others, 2002; VanLooy and others, 2006).

To assess whether corresponding features are co-located in the two images, the IFSAR DEM is resampled to the NED DEM grid cell size ($\sim$45 m), and the DEMs are differenced for preliminary analysis. The resulting difference map reveals significant disagreement ($\pm$300 m) between elevations of corresponding unglacierized grid cells in areas of steep ridgeline topography. Glacierized grid cells in the same areas reveal differences of the same order of magnitude, likely indicating a horizontal offset, since we do not expect such high rates of mass change at these elevations. However, across the full 80 km x 20 km scene, no single aspect shows consistent positive or negative discrepancies, indicating that the offset is non-linear. We further verify this using the image processing software ERDAS IMAGINE, which locates tie points – or topographically similar points – within each image, and determines the x and y offsets between the locations in each DEM. All glacier ice must be masked out, as glacierized areas are expected to show legitimate changes between the two map dates. Unfortunately, due to the extensive glacier coverage and discontinuous bedrock terrain in the scene, the number of robust tie points identified by the program

(∼200) is low for an image of this size and resolution. Moreover, the tie points themselves reveal inconsistent horizontal offsets, with a mean x and y offset between all points of approximately zero (indicating both negative and positive offsets that effectively cancel out when averaged). Together, the scarcity of quality tie points and the non-linear horizontal offsets between them indicate that the DEMs are not well co-located.

We attribute these offsets to error within the NED DEM. Significant offsets are known to exist for the NED (Arendt and others, 2002; Larsen and others, 2007), particularly in areas of steep terrain, as is the case in the Central Alaska Range. These are largely due to poor ground control of the pre-Global Positioning System era, which leads to photogrammetric error (Sapiano and others, 1998; Arendt and others, 2002, 2006; Larsen and others, 2007). Glacier accumulation areas are also particularly prone to error, due to poor image contrast resulting from featureless snow cover.

We discount the option of applying a polynomial fitting correction to the NED DEM to co-locate it with the high-quality IFSAR DEM, given the low number of quality tie points. Instead, we next consider statistical filtering options for eliminating the erroneous data. We begin by examining the distribution of surface height changes, and find that the histogram is strongly non-Gaussian (Fig. 2.8). This precludes the use of a standard 2σ filter. Instead, we test two additional filters based on the interquartile range, though we first exclude values from all grid cells with elevation <900 m, in order to preserve highly negative values in the ablation area which we attribute to real mass losses associated with several decades of increasing air temperatures. From the adjusted histogram without the low-elevation values, we eliminate outliers, defined as values falling outside of either:

$$Q_1 - 1.5 * (IQR) \tag{2.2}$$

or

$$Q_3 + 1.5 * (IQR) \tag{2.3}$$

where $Q1$ and $Q3$ are the first and third quartile, and IQR is the interquartile range. Unfortunately, we find this filter fails to remove substantial portions of the highly negative and positive values along the ridgelines. Imposing a stricter threshold and eliminating all values outside of the IQR-defined mid-fifty, however, means sacrificing large areas of the main glacier trunk that we do not suspect to be erroneous. We therefore discount these statistical filters.

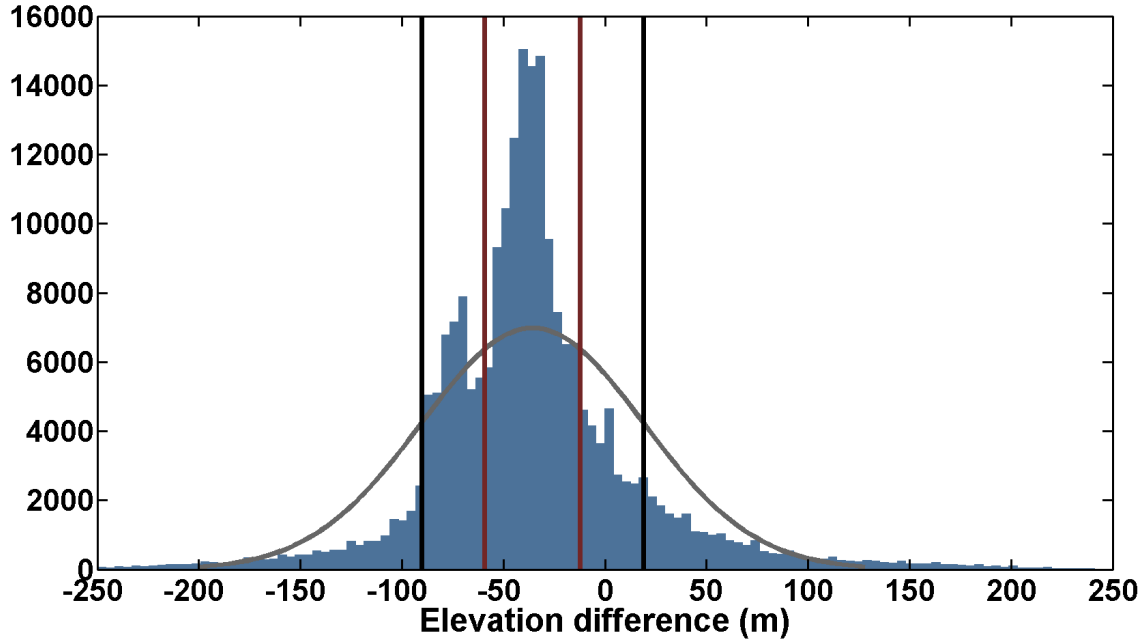

Figure 2.8. Distribution of uncorrected DEM difference map values. The grey curve is a Gaussian fit over the distribution, showing poor quality of fit. The standard deviation is bracketed by black lines, and the interquartile range is bracketed by red lines.

We finally choose a simple slope-dependent filter, whereby all grid cells with slope > 20° are masked out. We select this cutoff based on visual inspection, finding that the 20° slope threshold performs best at targeting erroneous values in steep zones while preserving areas along the main glacier trunk that we do not suspect to be problematic. Filtered grid cells represent 20% of the total glacier area for which we have IFSAR DEM data (Fig. 2.9).

Once this filter has been applied, masked-out portions are set to zero to maintain our ability to calculate glacier-wide balances for comparison to our other methods. Values in the northernmost portion of the glacier, where we lack IFSAR DEM data, are also set to zero. Surface height differences are integrated over the full glacier area, and converted to water equivalent units using a density of 850 $\pm$60 kg m^{-3}. The resulting glacier-wide balance represents losses between 1951 and 2011, which we divide by 60 years to get the annual balance rate.

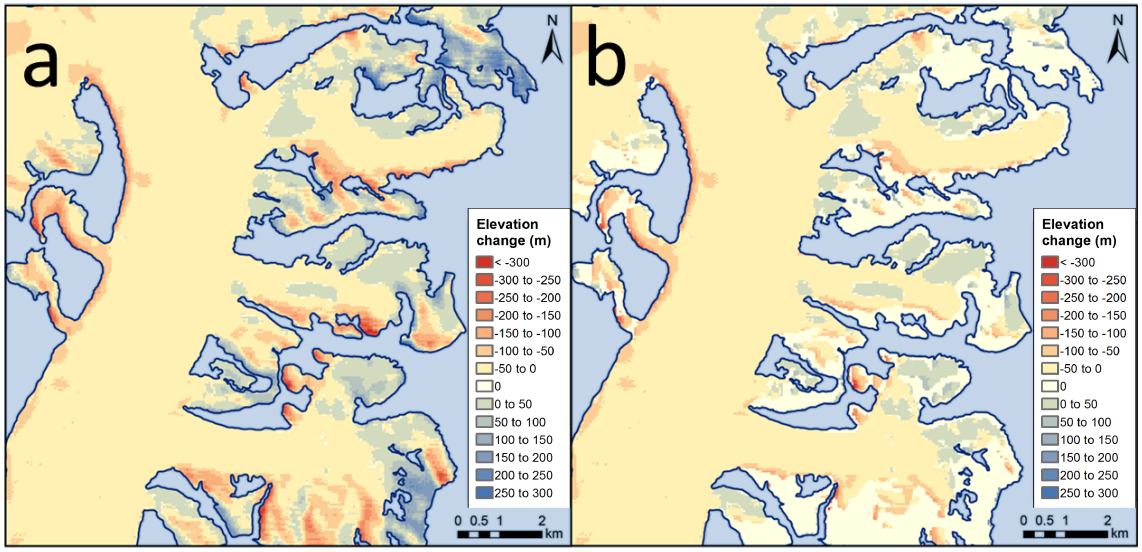

Figure 2.9. Quality control method for filtering erroneous values from DEM difference map. a) a zoomed-in portion of the central portion of the glacier, with highly negative and positive values visible in the steepest portions of the tributaries, near the ridgelines. b) the same area with a slope threshold applied, whereby the surface height changes of all grid cells with slope greater than 20° are set to zero.

2.2.2.3 Satellite gravimetry

The Gulf of Alaska solution outlined in Luthcke and others (2013) includes spatial and temporal constraints enabling a detailed uncertainty assessment over the entire region. Although no constraints are applied at the resolution of individual mascons, which limits uncertainty assessment at these spatial scales, several studies have found good agreement between altimetry and GRACE mascons summed over mountain regions (Arendt and others, 2008; Johnson and others, 2013). Here we follow a similar approach, choosing the Central Alaska Range mascon in which the Kahiltna Glacier is located (Fig. 2.10). The Luthcke and others (2013) solution provides a time series of cumulative mass balance for the entire Central Alaska Range mascon. To determine annual balances, we difference successive annual minima from the time series (Fig. 2.11). We then scale these mass changes by the ratio of the Kahiltna Glacier area to all glacier ice contained within the mascon (∼16%) and convert from Gt to meters water equivalent, to get annual balances for the Kahiltna Glacier basin alone.

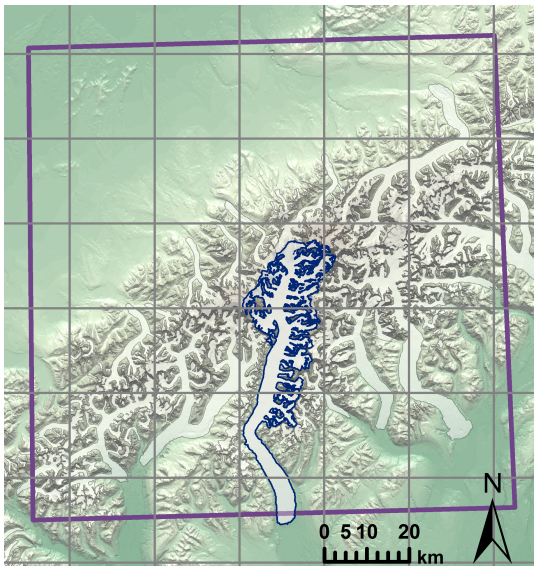

Figure 2.10. Location and relative size of the Kahiltna Glacier within the Central Alaska Range GRACE mascon. The Kahiltna Glacier basin is outlined in blue, and constitutes ~16% of the Central Alaska Range glacierized area contained within the mascon, shown in white. Grid spacing is 10 km.

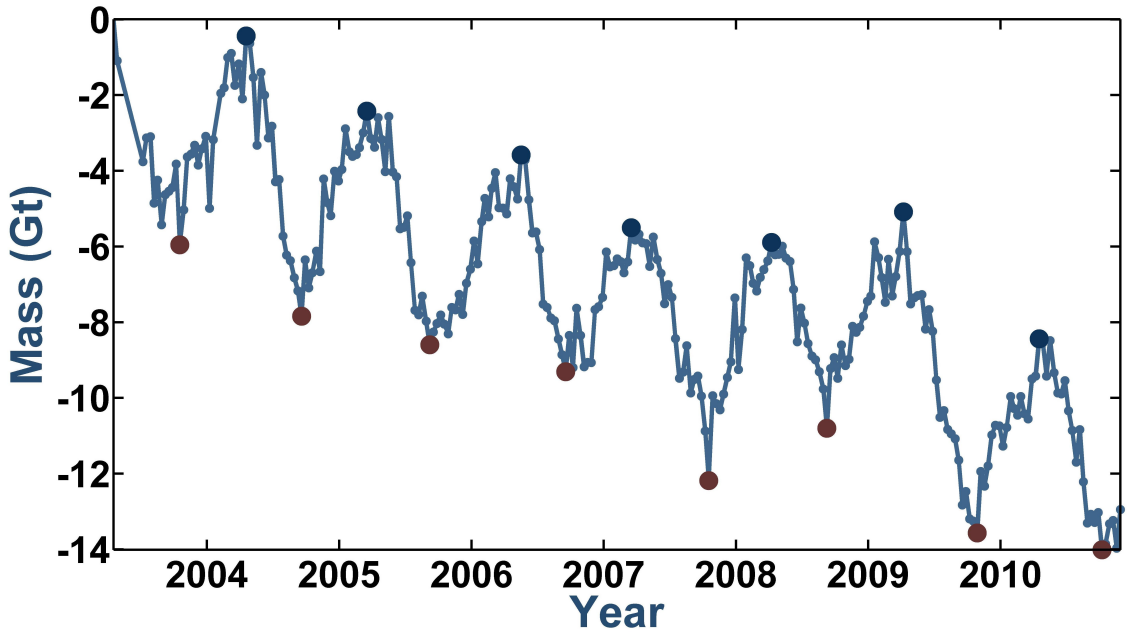

Figure 2.11. Cumulative mass balance derived from GRACE gravimetry for the Central Alaska Range mascon (Luthcke and others, 2013). The temporal resolution of GRACE observations is ~10 days. Annual mass balances are calculated by differencing successive annual minima (red).

2.3 Error analysis

2.3.1 Model

To test model sensitivity to our chosen values for the precipitation threshold temperature and melt factor for debris-covered ice, we carry out model simulations over a range of values for each variable: 0 to 2 °C and 0.7 to 1.3 mm day^{-1} K^{-1}, respectively. These represent the ranges typically explored in similar modeling studies. We test the effects of changing these parameters mainly on the mean annual balance derived from our five best optimized parameter sets, while also noting the effect on RMSE and R^2 values. We find the effect of precipitation threshold to be minimal across the range tested, causing very little change to RMSE, R^2 or annual balance estimates ($\pm$ -0.01 m w.e. yr^{-1}). We find the role of debris cover to be non-trivial, changing the annual balance by up to $\pm$ -0.28 m w.e. yr^{-1} ($\pm$ 23%)(RMSE and R^2 remain unchanged, as none of our actual mass balance stakes were located in debris-covered ice). Unfortunately, we lack sufficient in-situ data to fully characterize the debris cover on the glacier, making the effect of debris on melt rates one of our greatest sources of uncertainty.

When comparing modeled results to our observed mass balance measurements at the stake locations, we find that the largest discrepancy lies in the mass balance gradients with elevation. Typically, a lack of agreement between modeled and observed gradients prompts an adjustment of the lapse rate parameter. However, we employ actual measured lapse rates at each time step, as described in Sec. 2.1.1.4. Any error in lapse rates would therefore have to be from either a faulty temperature sensor or an over- or underestimation of lapse rates due to our issues with maintaining consistent sampling heights above the ice surface at all five sensors. To test the model sensitivity to these possibilities, we first employ a bootstrapping method to eliminate each sensor one at a time, recalculating lapse rates at every time step for the remaining four sensors. We find the effect on annual balance calculations for this test to be minimal (-0.05 m w.e. yr^{-1}, or within 5%), and the effect on R^2 to be very small. RMSE values increase from 0.65 m w.e. yr^{-1} to as high as 1.94 m w.e. yr^{-1}, though this is expected, given that the tuning parameters are optimized for model simulations that include all temperature sensors. We conclude that this first test reveals no reason to discard any one of the five temperature sensors employed in our hourly lapse rate calculations.

Second, we test the effects of adjusting the lapse rates at every time step by -0.2, -0.1, +0.1 and +0.2 °C km^{-1}. This type of adjustment could be necessary if our logarithmic profile corrections (Sec. 2.1.1.4 and A.2.1) were not sufficient to eliminate the effects of varying sensor heights above the surface (see Sec. 2.1.1.4). Results indicate that a change in lapse rate in either the positive or negative direction results in a more negative glacier-wide annual balance estimate in both cases; a change of -0.2 and +0.2 °C km^{-1} respectively yield a -0.18 m w.e. yr^{-1} ($\sim$15%) and -0.26 m w.e. yr^{-1} ($\sim$22%) change in mass balance. In other words, our optimized tuned model simulations produce not only a minima in RMSE, but also a minima in annual balance. This is explained because an increase in lapse rates produces a steeper modeled melt gradient than observed, exposing a vast amount of glacier area at elevations below our calibrating stake network to higher rates of melt. Conversely, a decrease in lapse rates produces a lower modeled balance gradient which, although it reduces melt rates, exposes a higher proportion of the glacier surface area to melt. More detailed analyses would have to be carried out to determine if a smaller change in lapse rate could reproduce our observed gradients exactly. We conclude that this cannot be excluded as a possible source of error. However, we also note that a lack of agreement between modeled and observed balance gradients could be a result of some other energetic process at the ice surface of this glacier that is simply not captured well by an air temperature proxy. In other words, though we cannot exclude the possibility of a lapse rate offset, another explanation for the discrepancy in balance gradients might also be possible.

Note that we consider the two different sensitivity tests involving lapse rates to incorporate the measurement error of the HOBO temperature sensors (reported as $\pm$0.21°C for temperatures above 0°C). If treated as a random error, the total effect of propagating this across 5 temperature sensors sampling at 10-minute intervals becomes minimal when calculating hourly lapse rates for use as model input. Treating the errors as systematic yields the same effect as adjusting the lapse rate by a set value, which is one of the sensitivity tests described above. We therefore do not include a separate error term to address the sensor measurement error.

To determine the total error, we propagate all errors in quadrature, including the RMSE calculated for our optimized 2011 simulation (Table 2.3). We consider this the error associated with our annual balance estimate for any one year, with the exception of 2010, for which we have a separate RMSE value. In order to bracket the uncertainties associated

Table 2.3. Summary of errors associated with modeling approach.

Error Component	Magnitude
RMSE (2010)	±0.62 m
RMSE (2011)	±0.65 m
Sensitivity to precipitation threshold parameter choice	±0.01 m
Sensitivity to melt factor for debris cover parameter choice	±0.28 m
Sensitivity to 'bootstrapping,' or removing one temperature sensor	±0.05 m
Sensitivity to lapse rate change	±0.26 m

with multi-year periods, we first treat uncertainties for each year as totally correlated. This yields a value for the maximum uncertainty. Conversely, we evaluate the minimum uncertainty by assuming that the errors are fully uncorrelated. We report the average of the two extremes, following similar methods in Motyka and others (2010).

As has been addressed in other studies (Radić and Hock, 2011), there are also other sources of error in glacier mass balance modeling that are difficult to quantify by standard error analysis or by sensitivity tests. For example, our model results are sensitive to our choice of supplementary climate data, both in terms of precipitation products (PRISM for spatial distribution and NCEP-NCAR for snowfall event magnitude and timing) and air temperature (NCEP-NCAR). Uncertainty associated with the use of these products is challenging to quantify formally, particularly given that we adjust the products to on-glacier conditions, and extrapolate from point locations to the entire glacier. We also recognize the uncertainty associated with the use of our in-situ stake measurements for calibrating the model. The Kahiltna Glacier ablation area has substantial surface ice undulations (i.e. height differences between adjacent peaks and troughs on the ice), which can have a considerable effect on stake measurements; during our field campaigns in 2011, three stakes at the same elevation and within ∼20 m of each other saw discrepancies in annual balances of up to 1.1 m w.e. This is not to say that any one stake measurement was incorrect, but instead that there is uncertainty associated with one stake's representativeness of a broader area and/or elevation (Cogley, 1999). Quantifying this would require an extensive network of stakes at every location, for the purpose of averaging the measurements. Due to

the logistical and financial expense of such a field campaign, we have not quantified this uncertainty in this study. In short, we acknowledge that as well as the calculated error values associated with parameter choices and potential errors in temperature data input, there is additional uncertainty that we are not able to quantify formally.

2.3.2 Remote sensing techniques

2.3.2.1 Airborne laser altimetry

Error for the airborne laser altimetry balance estimates are derived according to published methods (Larsen and others, 2007; Arendt and others, 2008; Johnson and others, 2013). The dominant source of measurement error of the altimetry method is associated with positioning the aircraft with the GPS-INS solution (King, 2009), which can lead to a net vertical and horizontal error of ± 0.2 m. This is empirically-derived through repeat surveying of fixed objects in Johnson and others (2013), in good agreement with earlier studies (Echelmeyer and others, 1996; Arendt and others, 2008; King, 2009). Uncertainty is also introduced when modeling dh/dt versus elevation, with a typical value as high as ± 1.0 m yr^{-1} at the uppermost and often steepest portions of the glacier where data is difficult to acquire. Note that this modeled dh/dt error may not be symmetric about the dh/dt profile, related to the fact that the upper and lower quartiles of the profile are taken about the dh/dt median, not the mean. Additional uncertainty enters when extrapolating the modeled dh/dt profile to the full glacier extent, and there is also often uncertainty associated with quantifying the glacier area itself. Finally, the assumption of a constant bulk density for the material gained or lost can result in a difference of up to 10% between balance values, depending on the choice of density value assumed.

These five uncertainties are propagated in quadrature sum to estimate the mass change error associated with the Kahiltna Glacier annual mass change estimates for each of the three available time periods from laser altimetry. Errors for the fourth period are derived separately in Arendt and others (2002). For the period spanning from 1951 to 2010, for which we do not have detailed analysis but for which we derive an estimate by combining our 1951 to 1994 and 1994 to 2010 estimates, we calculate a weighted mean from the errors associated with each of those two periods.

2.3.2.2 DEM differencing

Previous studies have used a number of different methods to quantify error of mass balance estimates from DEM differencing, ranging from simply treating the point uncertainty at every grid cell as completely correlated across the scene (Cox and March, 2004; Larsen and others, 2007), to treating them as uncorrelated (i.e. totally random) (Rignot and others, 2003; Thibert and others, 2008). These two options essentially represent the maximum and minimum possible error bounds, where the latter method is smaller than the former by a factor of $n^{1/2}$, with n being the number of grid cells. Some studies have also followed an intermediate approach using variograms to establish a correlation length between DEMs over bedrock areas (Rolstad and others, 2009; Motyka and others, 2010; Trüssel and others, 2013), which is then assumed as a measure of error correlation over ice. Yet this method depends on the availability of unchanging and unvegetated bedrock data adjacent to the glaciers.

Unfortunately, given the non-linear offset between different areas of bedrock in different corners of our 80 km x 20 km DEM scenes, we discard the method that uses an intermediate correlation length because of its dependence on unchanging bedrock data. Instead, we treat all point uncertainties as fully correlated, to establish the upper error bound. Following methodology developed by Larsen and others (2007) for an area of Alaska with similar NED quality issues, we determine all the sources of random and systematic error and propagate these by quadrature. For the NED DEM, we assume an uncertainty of $\pm$15 m for the ablation area and $\pm$30 m in the accumulation area, corresponding to one half and one full contour interval (Larsen and others, 2007).

Vertical RMSE values associated with the 2011 IFSAR DEM are relatively low, with values of 1.57 m for points with slope < 10%, and 5.12 m for slopes between 10% to 20% (Mantey, 2012). These values, however, are based on comparison with only 7 and 2 ground control points in each respective category, and may be subject to refinement with further product development. For lack of other data, we conservatively assign the RMSE of 5.12 m to all other slopes in the DEM, constituting 18% of the glacier surface area.

Finally, we also assume an uncertainty in our glacier area of 10%, following Arendt and others (2006) and Radić and Hock (2011), and an uncertainty in our assigned bulk density

Table 2.4. Summary of errors associated with DEM differencing method.

Error Component	Magnitude
NED DEM ablation area contour error	$\pm$15 m
NED DEM accumulation area contour error	$\pm$30 m
IFSAR DEM RMSE for slope < 10%	$\pm$1.57 m
IFSAR DEM RMSE for slope > 10%	$\pm$5.12 m
Error in assumed bulk density	$\pm$60 kg m^{-3}
Error in glacier area	$\pm$10%

value of $\pm$60 kg m^{-3} (Huss, 2013). Formal propagation of all of these uncertainties (listed in Table 2.4) in quadrature yields our final error estimate, which represents the maximum error we would expect.

To test our error estimate, we then analyze the distribution of elevation differences over non-ice-covered areas, following Larsen and others (2007). We find that the mean value is non-zero (4.6 m), indicating that despite correcting for the vertical datum difference between the NED (NGVD29) and IFSAR (NAVD88) DEMs, a vertical offset remains. We also find the distribution of elevation differences to be strongly non-Gaussian, meaning that the use of standard deviation as an estimate of the data spread is not valid (Fig. 2.12). Instead, we look at the interquartile range (IQR) as a possible estimate of the errors associated with differencing the two DEMs. Though Larsen and others (2007) find good agreement between the IQR value of their distribution and the formally calculated error value for their Southeast Alaska case, we find a large discrepancy for the Kahiltna Glacier area (the IQR value is nearly a factor of 6 larger than the formal error). We consider this to be additional evidence for the poor quality of the NED DEM, including over bedrock areas, further justifying our treatment of errors as fully correlated across the scene.

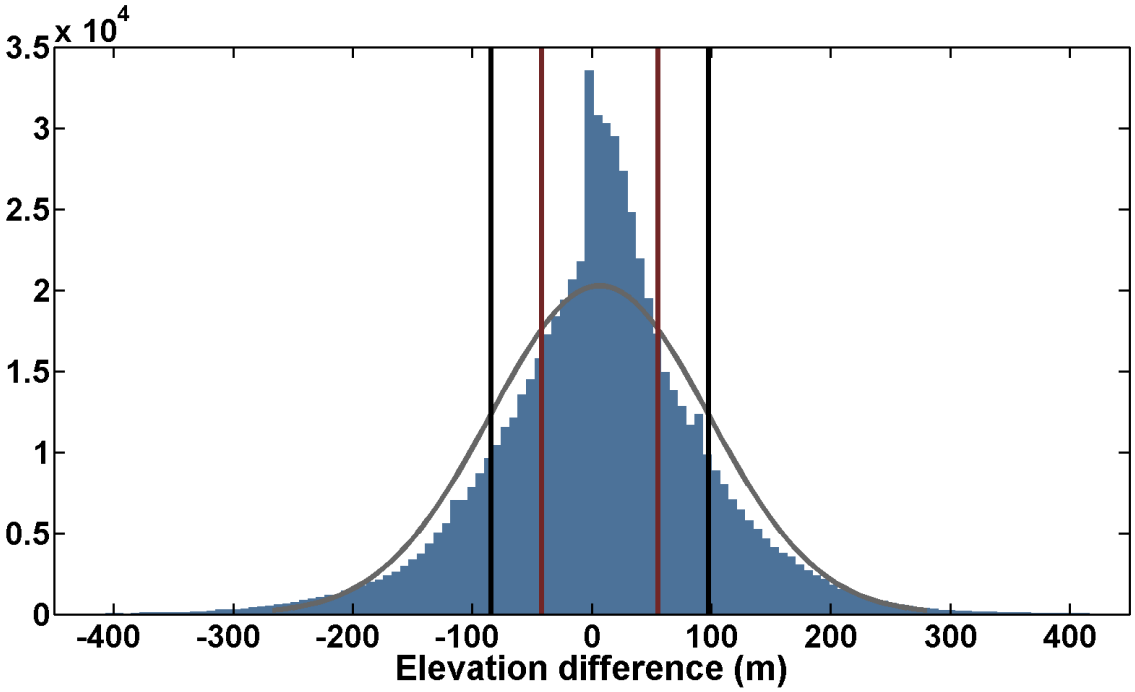

Figure 2.12. Distribution of DEM difference map values for non-glacierized bedrock terrain. The grey curve is a Gaussian fit over the distribution, showing poor quality of fit. The standard deviation is bracketed by black lines, and the interquartile range is bracketed by red lines.

2.3.2.3 Satellite gravimetry

Estimating error on our GRACE gravimetry mass balance estimates is difficult at the scale of individual mascons, due to smearing of the mass change signal between adjacent 1° x 1° mascons. We take a simple approach using the total error determined by Arendt and others (2013) for 2003 to 2010 mass loss estimates for the entire Gulf of Alaska, which we scale to the proportion of ice contained within the Central Alaska Range mascon alone. Arendt and others (2013) report mass changes for all Gulf of Alaska glaciers, representing an ice-covered region of 82,505 km^2. The Central Alaska Range mascon contains 3235 km^2 of glacier ice, or 3.9% of the total Gulf of Alaska ice area. We therefore take the associated fraction of their total reported error for the Gulf of Alaska as representative of the error associated with the Central Alaska Range alone for 2003 to 2010.

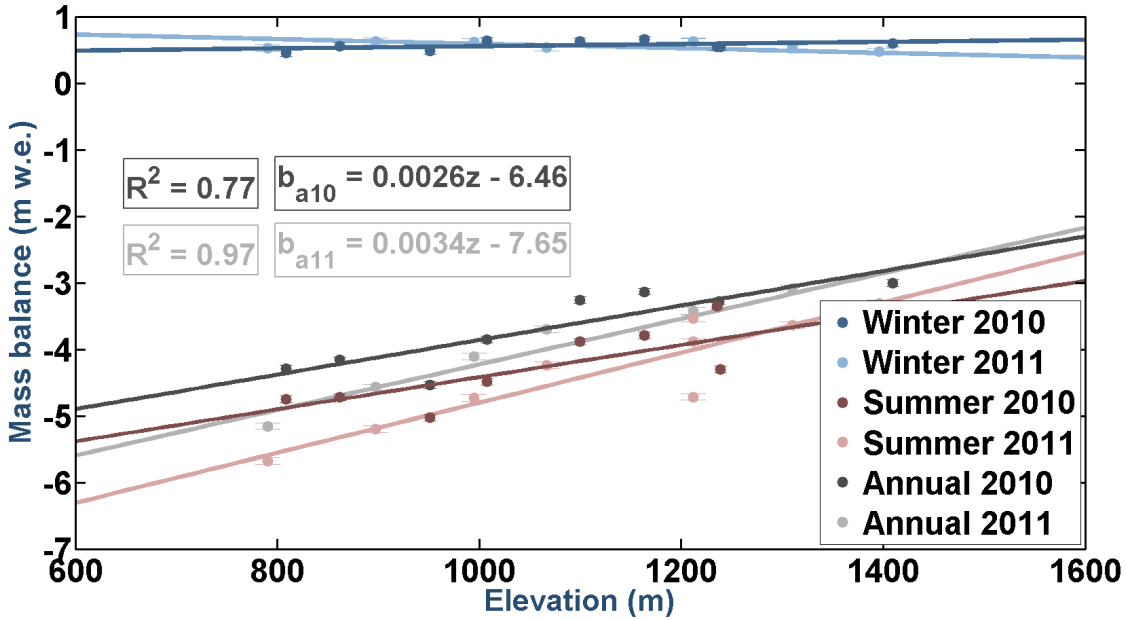

Figure 2.13. Observed 2010 and 2011 mass balance gradients.

2.4 Results and discussion

2.4.1 2010 to 2011 observations

Measured point annual balances for both 2010 and 2011 are approximately linear (Fig. 2.13). Though winter balance across the elevation range sampled shows large variability and no significant trend, summer balance dominates the linear trend, particularly since our observations are confined to a small elevation range (~600 m) in the ablation area where annual point mass change is mostly due to summer losses. Annual balance gradients differ between the two years, where 2010 shows a weaker gradient than both 2011 (0.0026 meters w.e. per meter elevation versus 0.0034 meters w.e. per meter elevation) and is lower than the value measured by the NPS (0.0032 m w.e. per meter elevation; see Sec. 1.1.2) (Mayo, 2001; Burrows and Adema, 2011). This may be due to the fact that, as previously mentioned, 2010 was generally observed to be a year of smaller than normal mass losses in Alaska (as is visible in the GRACE time series; Fig. 2.11).

Seasonal air temperature patterns are fairly typical of other on-glacier records, showing damped seasonal amplitudes resulting from the 0°C ice surface boundary condition in the

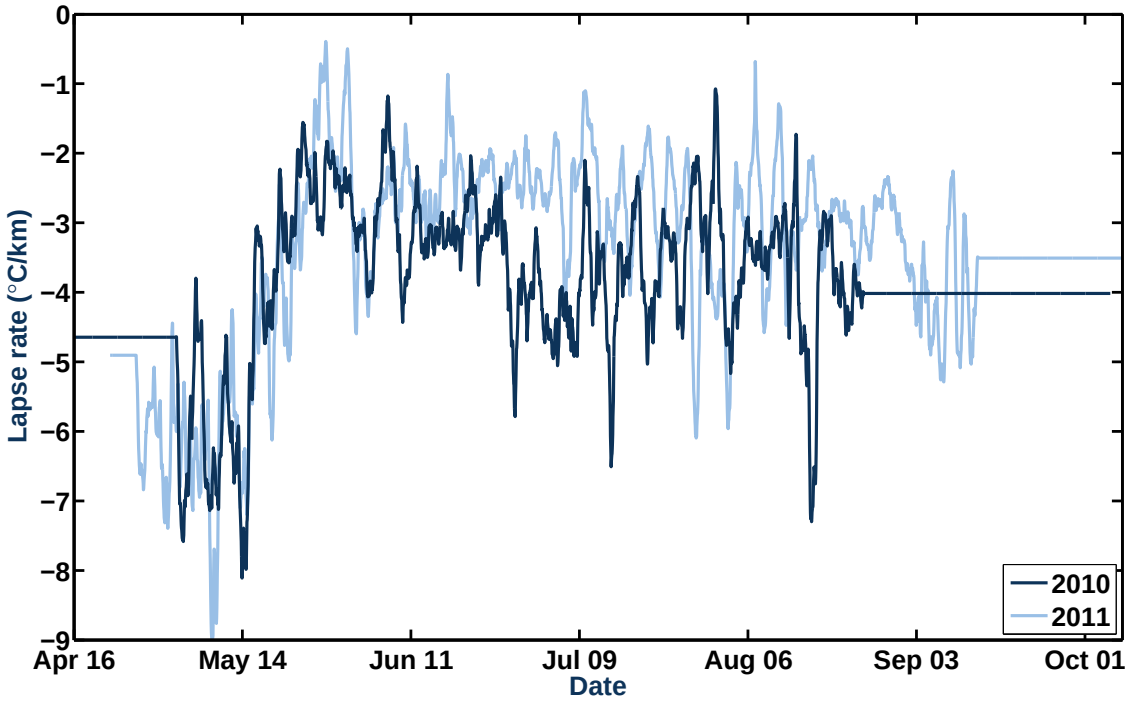

Figure 2.14. Time series of lapse rates used as model input for both 2010 and 2011 calibrating model simulations.

summer (Oerlemans, 2010). Lapse rate patterns across the elevations spanned are observed to be close to the environmental lapse rate in the early season of both years, becoming less negative later in the summer (Fig. 2.14). This agrees with typical on-glacier conditions (Oerlemans, 2010).

2.4.2 Model

2.4.2.1 2010 to 2011 simulations

Once we have determined the five best parameter sets optimized for reproducing melt recorded at our stakes between measurement dates, we then carry out model simulations for each year's full melt season to arrive at annual balances. By taking the mean of the five simulations, we derive best estimates of glacier-wide annual balance of -0.62 $\pm$0.73 m w.e. yr^{-1} for 2010 and -1.16 $\pm$0.76 m w.e. yr^{-1} for 2011. These values are substantially more

negative than the annual balances measured at the NPS index site, which are -0.41 $\pm$0.31 m w.e. yr^{-1} for 2010 and -0.61 $\pm$0.26 m w.e. yr^{-1} for 2011 (Burrows and Adema, 2011).

When comparing the resulting model output to our field observations, we find that modeled mass balance gradients between measurement dates (as opposed to annual balance gradients) are considerably steeper with elevation than those observed (0.0028 m w.e. m^{-1} modeled vs. 0.0021 m w.e. m^{-1} measured in 2010; 0.0030 m w.e. m^{-1} modeled vs. 0.0020 m w.e. m^{-1} measured in 2011). As a result, annual balance values are highly negative, since a large percentage of the glacier lies at low elevations, where melt is likely overestimated. Typically, a disparity between modeled and observed balance gradients indicates that the lapse rate parameter should be tuned. However, we employ actual measured lapse rates at each time step. From the results of the sensitivity analyses described in section 2.3.1, we do not suspect that any of the temperature sensors are faulty. We cannot eliminate, however, the possibility of an offset in lapse rates, and cannot confirm this without further on-glacier data collection.

2.4.2.2 Hindcasting

Using the five best parameter sets from our 2011 calibration model simulations, we drive the model with reanalysis air temperature and precipitation data from NCEP-NCAR (Sec. 2.1.1.4) for the period 1991 to 2009. Together with our independently-determined estimates from 2010 and 2011, we calculate a twenty-year average annual balance rate of -0.98 $\pm$0.47 m w.e. yr^{-1} (Fig. 2.17c). We also determine estimates for shorter time periods, for comparison to remote sensing techniques (Table 2.5).

When the Central Alaska Range glacier monitoring program was originally initiated in 1991, the NPS deemed the index site method as a plausible technique for estimating mass balances that are representative of the entire glacier from observations at a single stake (Ohmura and others, 1992; Mayo, 2001). To assess the representativeness of the NPS index site record over the 20-year measurement period, we compare the measured balances at the site to two model outputs: point balances at the same location, and specific glacier-wide balances (Figs. 2.15 and 2.16).

Table 2.5. Estimates of mass change derived from temperature index modeling for different time periods, for comparison to other methods.

Time period	Mass change (m w.e. yr^{-1})	Mean error (m w.e. yr^{-1})
1991 to 2011	-0.98	$\pm$0.47
1995 to 2008	-0.93	$\pm$0.48
1995 to 2010	-0.95	$\pm$0.49
2008 to 2010	-1.09	$\pm$0.65
2003 to 2010	-1.09	$\pm$0.54

We find that modeled and measured annual mass balance at the index site location are not strongly correlated (R^2 = 0.24). Separated into seasonal components, summer balances show slightly higher R^2 values than winter (0.16 versus 0.06), though both correlations are weak. Similarly, comparison between modeled specific glacier-wide mass balance and the index site measurements shows poor correlation for each annual, summer and winter balances (R^2 = 0.26, R^2 = 0.18 and R^2 = 0.06, respectively). When analyzed as cumulative balances (Fig. 2.16), we observe that the three records diverge significantly from one another. While the measured NPS index site mean balance is only slightly positive (0.15 $\pm$1.31 m w.e. yr^{-1}; (Burrows and Adema, 2011)), the model places the index site well into the accumulation area, yielding a substantially more positive mean balance value after the 20-year simulation (mean B_a = 0.98 m w.e. yr^{-1}). The modeled glacier-wide balance, on the other hand, is strongly negative (mean B_a = -0.98 $\pm$0.47 m w.e. yr^{-1}).

The lack of correlation between modeled results and measurements at the NPS index site may be attributable to issues with either method. These may include stake measurement errors, problems with the model's characterization of accumulation or melt, or some combination thereof. Though we acknowledge that the primary flaw of our model simulations is the failure to reproduce the balance gradient from our stake network, the difference in gradients should nonetheless not affect the correlation between measured and modeled balances from year to year. This points to the possibility that mass balance measurements at the index site may not be representative of fluctuations at the glacier-wide scale.

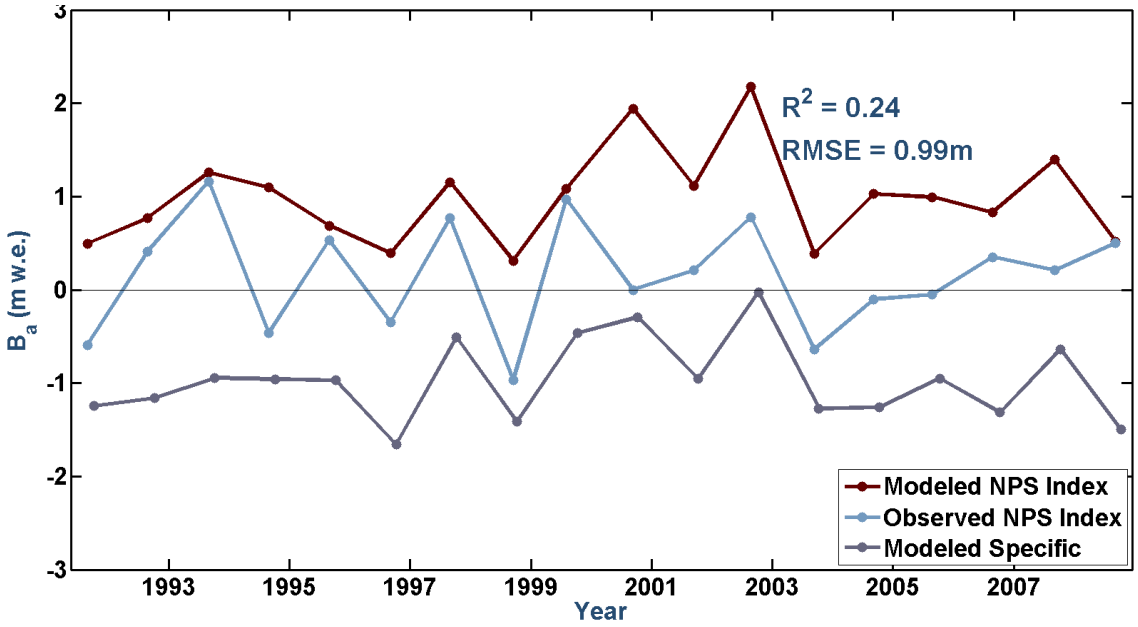

Figure 2.15. Modeled and observed annual point balance at the NPS index site from 1992 to 2011, with modeled annual glacier-wide (area-averaged) balance. R^2 and RMSE values for correlation between the measured and modeled NPS index site mass balances are given.

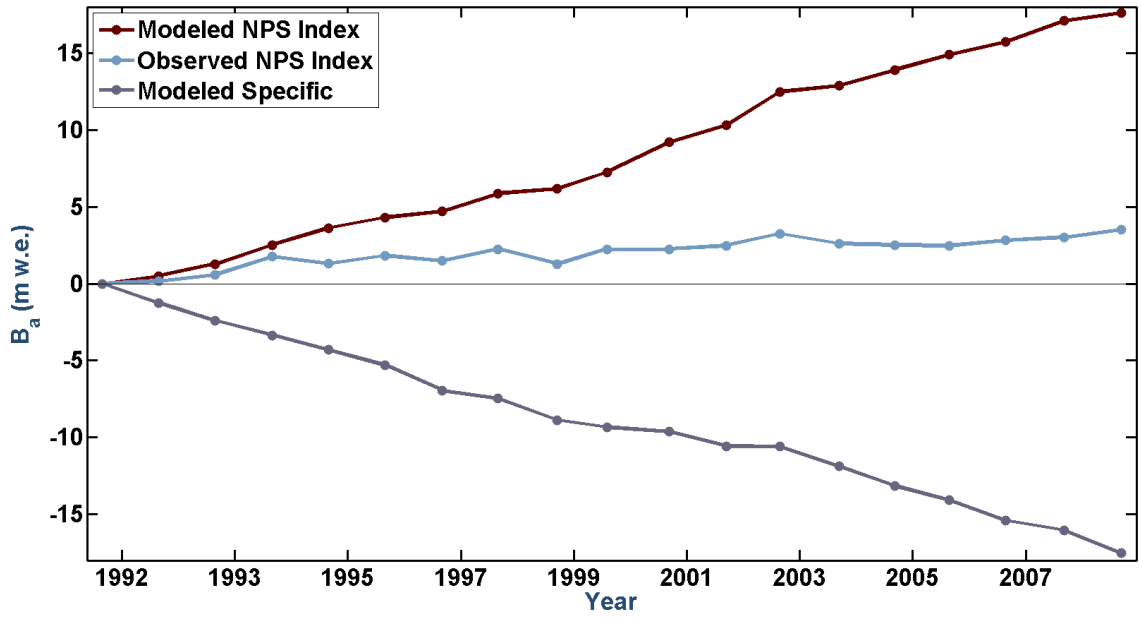

Figure 2.16. Modeled and observed cumulative annual point balance at the NPS index site from 1992 to 2011, with modeled cumulative annual glacier-wide (area-averaged) balance.

The estimate of mean annual balance we derive from our hindcasting simulations is quite strongly negative when compared to values from other methods (see sections below). This is likely attributable to the steepness of the modeled balance gradient which, while optimized to reduce the RMSE at the stakes in our relatively small measured elevation range, exposes a large portion of the ablation area to higher rates of melt than are likely. From our uncertainty analysis, we find that the model is highly sensitive to a change in lapse rate, suggesting that a systematic offset in our input lapse rate data could result in an overestimation of mass loss. Alternatively, the effect of debris cover on melt rates is another leading source of uncertainty, as the terminus is largely rock-covered (i.e. 71% covered below 900 m elevation) and we have limited in-situ measurements of debris thickness by which to assign the melt reducing factor in the model. An underestimation of melt suppression under debris could therefore contribute to our strongly negative modeled balances.

2.4.3 Remote sensing techniques

We next compare our model estimates to those derived from three remote sensing techniques.

2.4.3.1 Airborne laser altimetry

Using three laser altimetry profiles and one synthetic flight line extracted from the 1951 NED DEM, we compare mass loss values for four distinct time periods, and combine two of the estimates to cover the full time span (Table 2.6). We see evidence for accelerated mass loss within the most recent time periods. This agrees with a number of studies that have found notable increases in glacier mass loss since the 1990s (Dyurgerov and Meier, 2000; Arendt and others, 2002; Kaser and others, 2006; Zemp and others, 2009; Johnson and others, 2013), changes that are attributed to an increase in mean annual air temperatures (Serreze and others, 2000; Stafford and others, 2000; Overland and others, 2002; Hinzman and others, 2005).

Examining the mass changes between 1994 and 2010 (the longest time period between actual laser profiles) (Figs. 2.17b and 2.19), we observe significant rates of thinning over large portions of the ablation area. Areas that are particularly vulnerable to thinning are

Table 2.6. Estimates of mass change derived from airborne laser altimetry for different time periods. Note that a seasonal correction has been applied to 1994 data for comparison to 2008 and 2010, to compensate for the difference in acquisition dates.

Time period	Mass change (m w.e. yr^{-1})	Error (m w.e. yr^{-1})
1951 to 1994	-0.39	+0.09/-0.09
1995 to 2008	-0.68	+0.10/-0.09
1995 to 2010	-0.69	+0.07/-0.08
2008 to 2010	-1.01	+0.44/-0.37
1951 to 2010	-0.48	+0.08/-0.09

between 300 to 700 m and 1800 to 2200 m elevation; both of these ranges represent large, wide and flat portions of the glacier. Surface height changes at all elevations sampled (up to ∼3000 m) are exclusively negative, with extrapolated elevations up to ∼5000 m also showing signs of thinning. No zones of thickening are observed.

Comparing the mean annual glacier-wide mass balance from 1994 to 2010 with our model estimate for the same period, we see substantial disagreement between the values(-0.69 +0.07/-0.08 m w.e. yr^{-1} from laser altimetry versus -0.95±0.49 m w.e. yr^{-1} from the model). Though the values agree to within error bars, we propose that this disagreement is further evidence for an overestimation of mass losses as derived from the model.

2.4.3.2 DEM differencing

Next, DEM differencing provides an independent test for assessing estimates from the laser altimetry method, to inform whether the mass loss magnitudes we derive from laser altimetry represent the magnitudes we would hope to achieve in our model simulations. By differencing the historic NED and the modern-day IFSAR DEMs, we obtain an annual balance rate of -0.41 ±0.26 m w.e. yr^{-1} for the period spanning 1951 to 2011 (Figs. 2.17c). This agrees within error to the laser altimetry estimate of -0.48 +0.08/-0.09 m w.e. yr^{-1} for 1951 to 2010, derived by combining two estimates from consecutive time periods.

Comparing both the spatial patterns and the distribution of surface height changes from DEM differencing (Figs. 2.18 and 2.17c) to laser altimetry analyses from 1994 to 2010 (Figs. 2.19 and 2.17b), we see a strong similarity in thinning patterns, despite a difference in time period. These findings lend confidence to the elevation binning techniques employed in laser altimetry to extrapolate centerline profiles to the full glacier extent, an approach called into question previously by Berthier and others (2010), who compared DEM differencing estimates to those derived from a simulated laser centerline extracted from a DEM. Subsequent studies have nonetheless re-affirmed the validity of the centerline extrapolation techniques used (Johnson and others, 2013), and our findings provide strong additional support. Moreover, the close agreement between these methods suggests we can have confidence in the estimates of glacier-wide mass balance derived from laser altimetry as a means to assess our model performance.

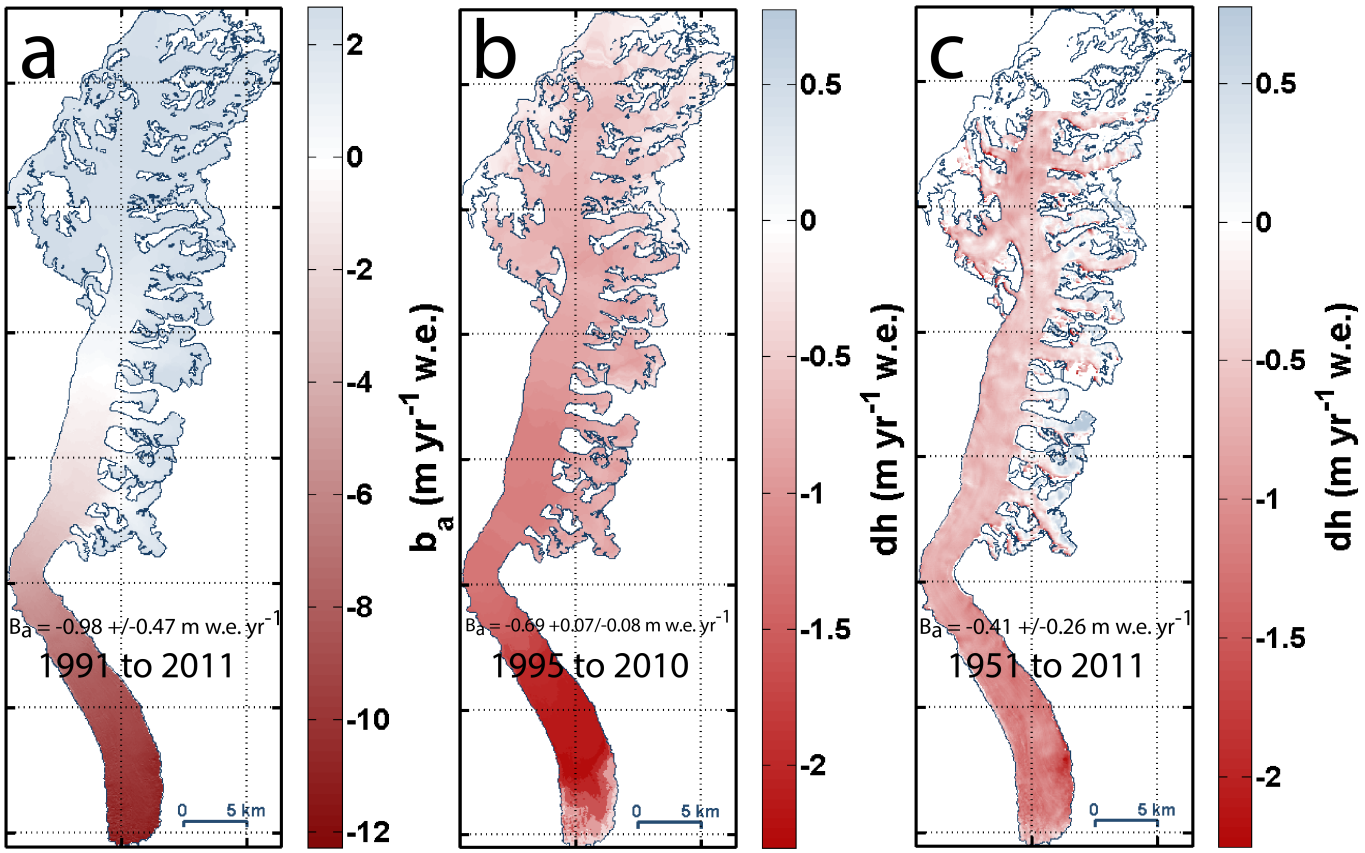

Figure 2.17. Comparison of spatial patterns of mass balance and surface height change from model, laser altimetry and DEM differencing. a) Average 1991 to 2011 modeled glacier-wide annual balance. b) Surface height change map for 1994 to 2010 derived from laser altimetry. c) Glacier surface height changes between 1951 and 2011 from DEM differencing. Note the different scale bars for the different methods, depending on whether the technique estimates spatially distributed mass balance or surface height change.

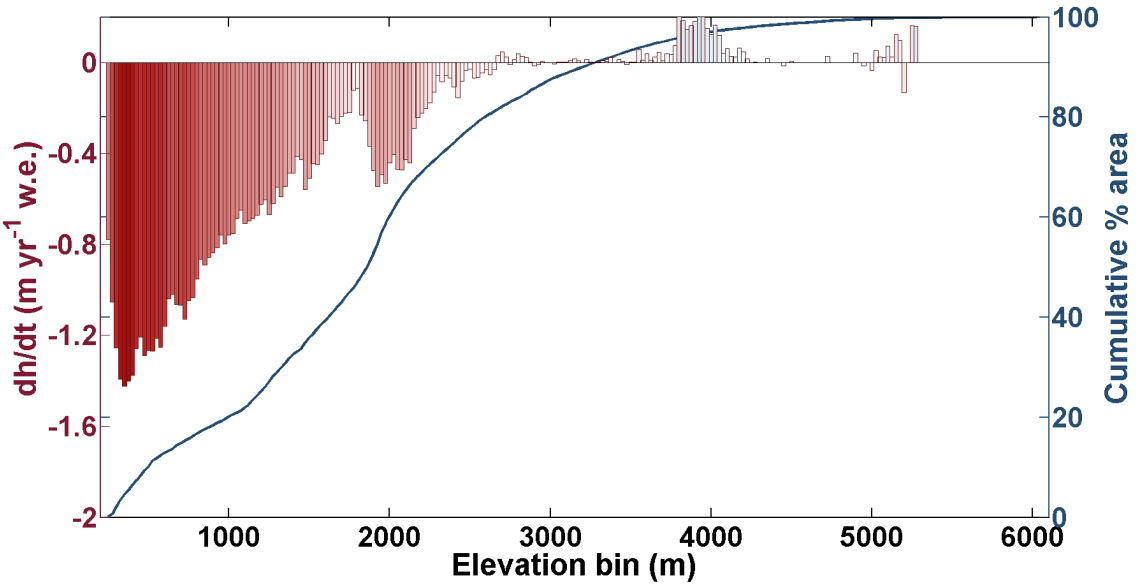

Figure 2.18. Glacier surface height changes between 1951 and 2011 as a function of elevation, derived from DEM differencing. The glacier's cumulative percent area with elevation is shown on the right-hand y-axis, to give an indication of which elevations are the most important in terms of areal extent.

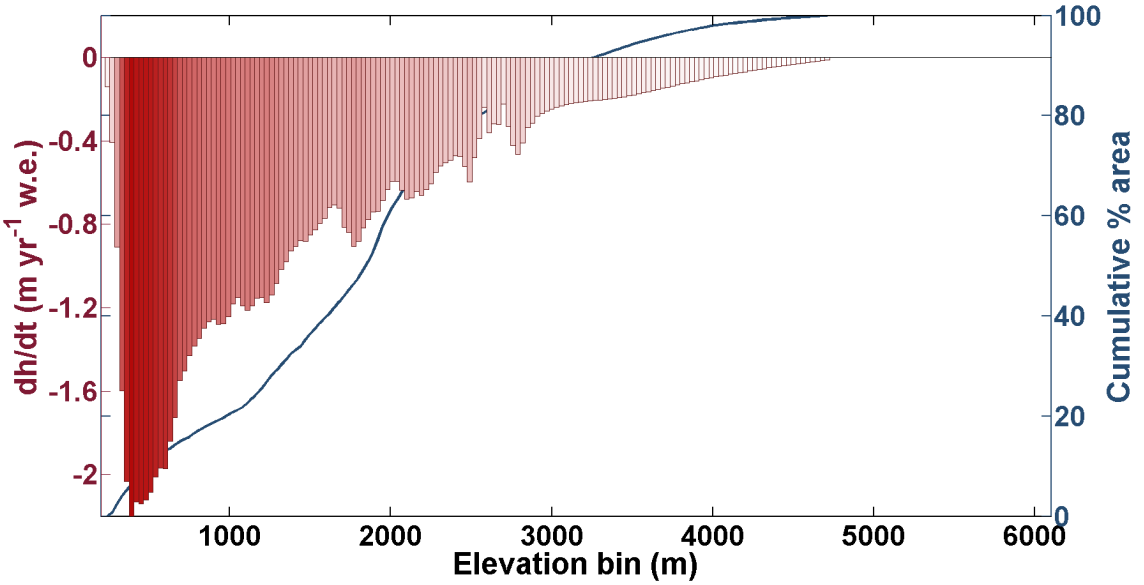

Figure 2.19. Glacier surface height changes between 1994 to 2010 as a function of elevation, derived from laser altimetry. The glacier's cumulative percent area with elevation is shown on the right-hand y-axis; ~85% of the glacier area lies at or below 3000 m, indicating good data coverage by the laser altimetry centerline.

2.4.3.3 Satellite gravimetry

Using data from the twin GRACE satellites, a time series of mass change derived for the Central Alaska Range and downscaled to the area of the Kahiltna Glacier reveals an average annual mass balance of -0.36 $\pm$0.13 m w.e. yr^{-1} for 2003 to 2010. This estimate is best compared to modeled values covering the same time period (-1.09 $\pm$0.54 m w.e. yr^{-1}) and to laser altimetry values for 1995 to 2010 (-0.69 $\pm$0.13 m w.e. yr^{-1}). Although our modeled results likely overestimate mass loss (as discussed in Sec. 2.4.2.2) and therefore do not allow for robust comparison, we suspect that the discrepancy between estimates from satellite gravimetry and the modern laser altimetry period indicates that this simple approach to GRACE downscaling underestimates mass loss. One possible explanation for this may be that in this approach, mass loss is simply partitioned by area for all glaciers within the Central Alaska Range, whereas the large, south-facing glaciers on the south side of the range (such as the Kahiltna Glacier) likely experience greater mass turnover than those on the north. This points to the possibility of developing a more sophisticated gravimetry downscaling method, where different zones of the mascon are weighted differently when partitioning the GRACE mass change signal. To date, other than the single NPS index site on the Traleika Glacier (Mayo, 2001; Burrows and Adema, 2011), insufficient in-situ observations exist for the north side of the range to constrain these zonal differences.

One of the benefits of the GRACE dataset is our ability to compare it to model output of individual annual balances (Fig. 2.20), as well as to the full time series of cumulative balance at a given stake location (Fig. 2.21). For the former, although the magnitudes of the estimates derived from GRACE are consistently less negative than those from the model, the variability between the two is well-correlated, yielding an R^2 value of 0.72. For the latter, we test the correlation between the time series from GRACE and the time series of cumulative mass balance at the NPS index site at 1925 m elevation (Burrows and Adema, 2011), both of which are linearly detrended to remove the long-term mass change signal in each record (Fig. 2.21). We find these to be reasonably correlated, with an R^2 value of 0.55. However, comparing GRACE to the time series from a different stake location (KT1), located at 1409 m elevation in the ablation area, we find notably better correlation with R^2 = 0.81. This is likely attributable to the elevation differences and, in turn, the stake's location

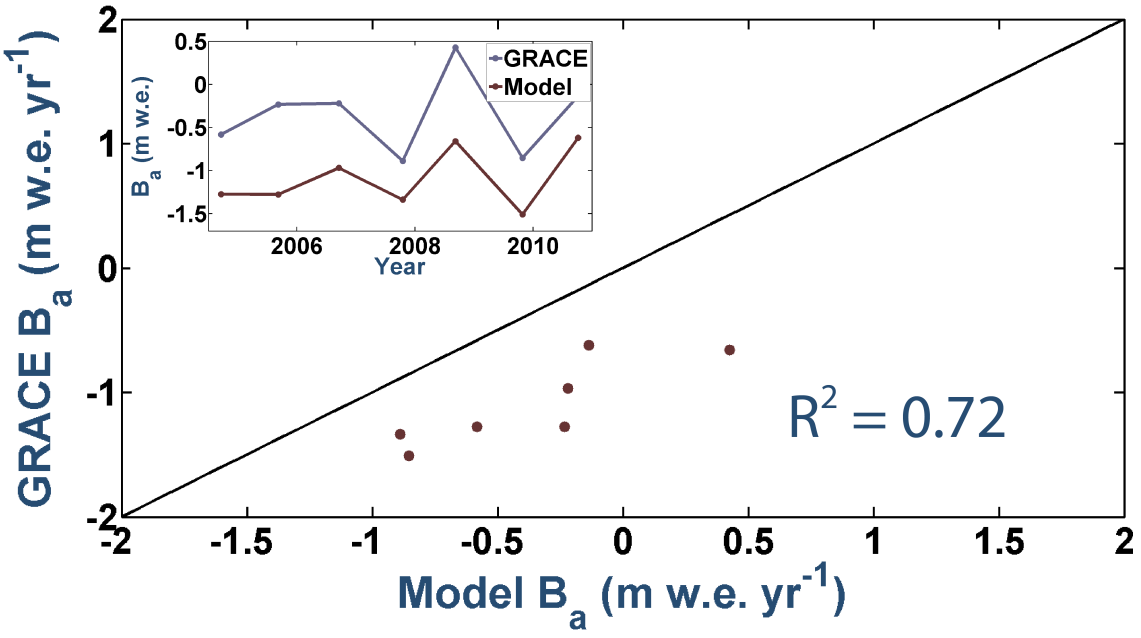

Figure 2.20. Comparison of GRACE-derived and modeled annual balances for 2004 to 2010. Main figure shows the scatter plot of annual balance estimates from GRACE versus those from the model, while the inset shows the estimates from each method as a time series.

in an ablation- or accumulation-dominated zone of the glacier. In other words, GRACE may be better correlated to areas of the glacier where the air temperature signal is the primary driver of subannual changes, rather than precipitation. This makes sense given the relatively large uncertainty associated with precipitation data from climate products as compared to air temperature data.

We believe that this significant correlation is strong evidence for the promising ability of downscaled GRACE to reveal much of the information about subannual and interannual variability that typically requires the application of a climate-driven mass balance model. With the ongoing development of methods for downscaling GRACE to smaller spatial scales, it is possible that GRACE may prove a useful tool for characterizing past and present temporal evolution of glacier mass changes without the need for meticulous model simulations. Our results point to the possibility of using gravimetry in tandem with bulk mass change estimates from laser altimetry and/or DEM differencing to obtain information on both seasonal and long-term mass changes.

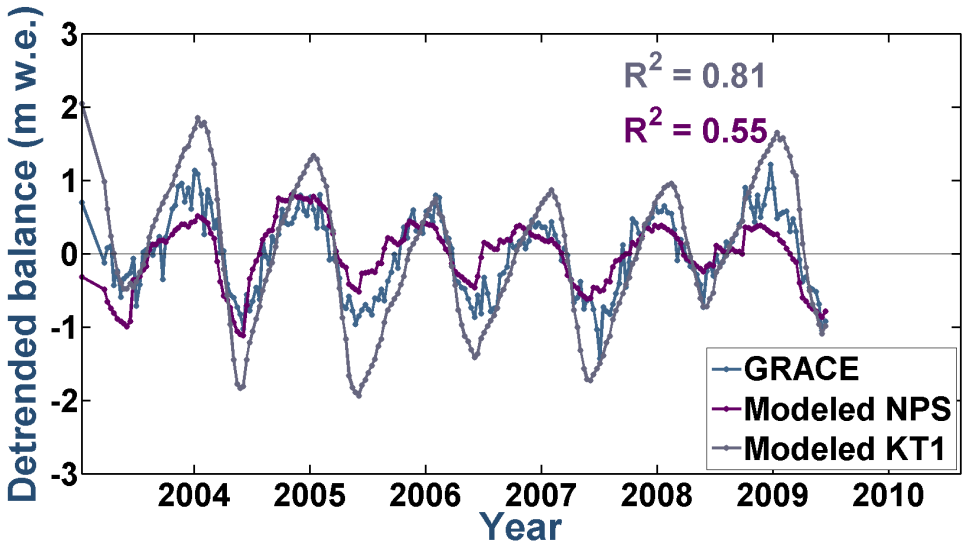

Figure 2.21. Comparison of GRACE time series to modeled index site and ablation area stake balances. The modeled time series for KT1, the ablation area stake at 1409 m is shown in grey, while purple designates the NPS index site stake at 1925 m. GRACE is shown in blue.

2.4.4 Mean mass balance estimates from all methods

Comparing all glacier-wide annual balance estimates derived from the four different methods, we see that all methods and all time periods reveal mass loss (Fig. 2.22 and Table 2.7). Strong evidence exists for mass loss acceleration since the 1990s, particularly visible in the laser altimetry estimates. Long-term estimates derived from laser altimetry and DEM differencing are in very close agreement, lending strength to the elevation-bin extrapolation techniques employed in laser altimetry, and subsequently to the estimates we derive from this method. The mean annual estimate we calculate from GRACE may be underestimating mass loss as it relates to the other methods, while the mean estimate from modeling may be too negative, and is bounded by a large degree of uncertainty.

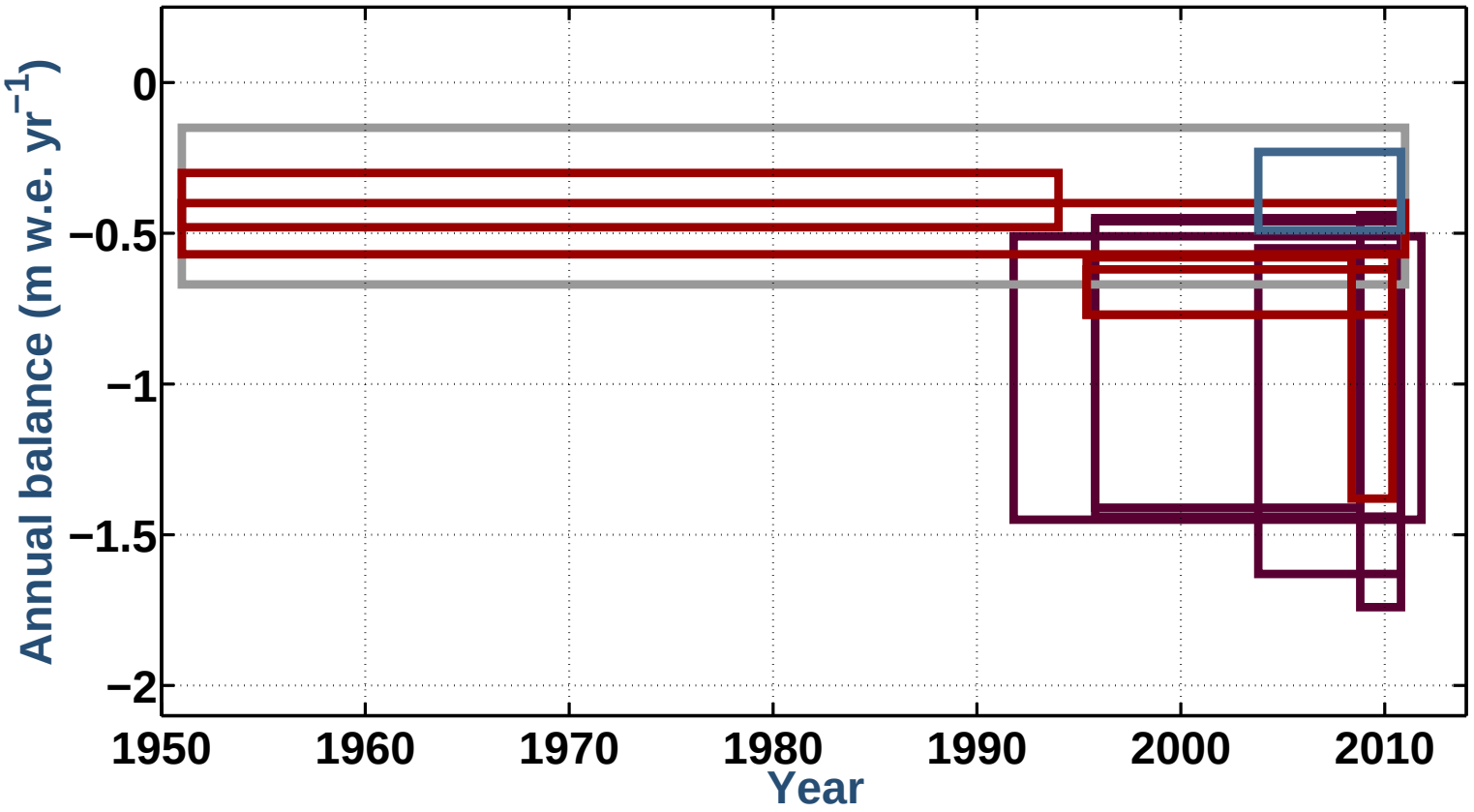

Figure 2.22. Box plot showing comparison of annual mass balance estimates from all four methods. Estimates are shown for all time periods for which we are able to calculate an annual balance rate. The width of the box represents the time spanned by the method, the center height indicates the estimated annual balance, and the total height of the box indicates the error on the annual balance value. Model estimates are shown in purple, laser altimetry in red, DEM differencing in grey, and GRACE gravimetry in blue.

Table 2.7. Estimates of mass change derived from all methods for all time periods.

Method	Time period	Mass change (m w.e. yr^{-1})	Error (m w.e. yr^{-1})
Model	1991 to 2011	-0.98	$\pm$0.47
	1995 to 2008	-0.93	$\pm$0.48
	1995 to 2010	-0.95	$\pm$0.49
	2008 to 2010	-1.09	$\pm$0.65
	2003 to 2010	-1.09	$\pm$0.54
Laser altimetry	1951 to 1994	-0.39	+0.09/-0.09
	1995 to 2008	-0.68	+0.10/-0.09
	1995 to 2010	-0.69	+0.07/-0.08
	2008 to 2010	-1.01	+0.44/-0.37
	1951 to 2010	-0.48	+0.08/-0.09
DEM differencing	1951 to 2011	-0.41	$\pm$0.26
Satellite gravimetry	2003 to 2008	-0.36	$\pm$0.13

Chapter 3

Conclusions

In this study, we derive mass balance estimates for the large Kahiltna Glacier in the Central Alaska Range using a temperature index model based on limited field data, and we compare results to those derived from three remote sensing techniques.

We begin by calibrating our model to field observations collected in 2010 and 2011, and hindcast for 20 years for comparison to National Park Service mass balance measurements at a single index site. Unfortunately, our model fails to reproduce the NPS time series of summer, winter and annual balances recorded, generating weak correlations between measurements and modeled results. Because of these poor correlations to temperature-driven modeling, and because the NPS index site shows a slightly positive long-term balance trend while we calculate consistent mass losses from all other methods, the index site is likely not representative of the glacier-wide mass balance regime.

We also compare modeled glacier-wide estimates to those from airborne laser altimetry for 1995 to 2010, and find our model balance estimates to be substantially more negative. To independently test the laser altimetry method, and to inform whether the mass loss magnitudes we derive from laser altimetry represent the magnitudes we would like to achieve in our model simulations, we compare laser altimetry estimates for 1951 to 2010 to those from DEM differencing for 1951 to 2011. We find close agreement, lending strength to the extrapolation techniques employed in laser altimetry, and pointing to mass balance estimates from this approach as robust constraints for our other methods.

Reviewing all glacier-wide annual balance estimates derived for all time periods using the four different methods, we find several points of agreement, and some disagreement. First, all methods and all time periods reveal consistent mass losses. Moreover, strong evidence exists for mass loss acceleration since the 1990s, especially visible in the laser altimetry record. We observe marked agreement between long-term mean annual estimates derived from both laser altimetry and DEM differencing. The model, however, likely overestimates mass losses, and our estimate from GRACE gravimetry is a likely underestimate.

In terms of uncertainty, laser altimetry yields the lowest errors, although density uncertainty creates larger errors over short time spans. DEM differencing is the next best option

for quantifying long-term changes, keeping in mind that though our error bars are large for this rugged portion of the Alaska Range, the availability of better quality historic DEMs could result in much smaller DEM differencing errors in other regions of Alaska. Finally, our temperature index model, with a parameter set calibrated to on-glacier mass balance measurements, has the largest associated error of any of the methods. This results from uncertainties in our input data due to extrapolations from limited field observations. In other words, the model is poorly constrained, and is also sensitive to parameter choices such as the melt suppression factor for debris, for which we have little in-situ data.

Though our temperature-index model likely overestimates mass losses, modeling has long been the conventional method for obtaining information on seasonal and interannual changes, and is very useful for hindcasting and forecasting at a desired temporal resolution. GRACE gravimetry is the only technique of the three remote sensing methods that does not simply yield a bulk mass change, but that has high temporal resolution, and that can be directly compared to the time-evolving mass balances from our temperature index model. We find strong correlation between both the annual glacier-wide mass balances ($R^2 = 0.72$) and the detrended time series of cumulative mass balance at an ablation area site ($R^2 = 0.81$). Correlation is not as strong to an accumulation area site, likely because of the greater uncertainty associated with precipitation datasets than with air temperature products. Nonetheless, we believe this strong correlation indicates the potential use of GRACE data for providing seasonal and interannual information.

We propose that the best approach for estimating seasonal and long-term balance trends for a field site with limited ground observations is to integrate several different techniques. Relying on mass balance modeling alone without adequate in-situ measurements yields a large degree of uncertainty that can nearly exceed the estimate itself. Integrating a mass balance model with geodetic observations from DEM differencing or laser altimetry, however, can place constraints on the magnitudes of mass changes the model should yield, while still providing information on seasonal and interannual changes. Alternatively, GRACE gravimetry is a tool that shows promising correlation to modeled mass changes at high temporal resolution. With ongoing refinement to downscaling methods and with further tests of GRACE's performance in other mascons and on other glaciers, it may be possible to extract seasonal information from gravimetry without the need for climate-driven model simulations.

References

Arendt, A., K. Echelmeyer, W. Harrison, C. Lingle and V. Valentine, 2002. Rapid wastage of Alaska glaciers and their contribution to rising sea level, *Science*, **297**(5580), 382–386.

Arendt, A., K. Echelmeyer, W. Harrison, C. Lingle, S. Zirnheld, V. Valentine, B. Ritchie and M. Druckenmiller, 2006. Updated estimates of glacier volume changes in the western Chugach Mountains, Alaska, USA and a comparison of regional extrapolation methods, *Journal of Geophysical Research*, **111**(F10), 03019.

Arendt, A., S. Luthcke, A. Gardner, S. O'Neel, D. Hill, G. Moholdt and W. Abdalati, 2013. Analysis of a GRACE global mascon solution for Gulf of Alaska glaciers, *Journal of Glaciology*, **59**(217), 913.

Arendt, A., S. Luthcke, C. Larsen, W. Abdalati, W. Krabill and M. Beedle, 2008. Validation of high-resolution GRACE mascon estimates of glacier mass changes in the St. Elias Mountains, Alaska, USA using aircraft laser altimetry, *Journal of Glaciology*, **54**(188), 778–787.

Bader, H., 1954. Sorge's law of densification of snow on high polar glaciers, *Journal of Glaciology*, **2**(15), 319–322.

Berthier, E., E. Schiefer, G. Clarke, B. Menounos and F. Rémy, 2010. Contribution of Alaskan glaciers to sea level rise derived from satellite imagery, *Nature Geoscience*, **3**, 92–95.

Burrows, R. and G. Adema, 2011. Annual Report on Vital Signs Monitoring of Glaciers in the Central Alaska Network, 2010, *Technical report*, National Park Service.

Burrows, R., S. Herreid, G. Adema, A. Arendt and C. Larsen, 2011. Glacier Trends and Response to Climate in Denali National Park and Preserve, *Technical report*, Park Science, National Park Service.

Campbell, S., K. Kreutz, E. Osterberg, S. Arcone, C. Wake, D. Introne, K. Volkening and D. Winski, 2012a. Melt regimes, stratigraphy, flow dynamics and glaciochemistry of three glaciers in the Alaska Range, *Journal of Glaciology*, **58**(207), 99–109.

Campbell, S., K. Kreutz, E. Osterberg, S. Arcone, C. Wake, K. Volkening and D. Winski, 2012b. Flow dynamics of an accumulation basin: a case study of upper Kahiltna Glacier, Mount McKinley, Alaska, *Journal of Glaciology*, **58**(207), 185–195.

Chen, G., 1998. GPS kinematic positioning for the airborne laser altimetry at Long Valley, California, PhD thesis, Massachusetts Institute of Technology.

Chen, J., C. Wilson and B. Tapley, 2006. Satellite gravity measurements confirm accelerated melting of Greenland ice sheet, *Science*, **313**, 1958–1960.

Cherry, J.E., S. Walker, N. Fresco, S. Trainor and A. Tidwell, 2010. Impacts of Climate Change and Variability on Hydropower in Southeast Alaska: Planning for a Robust Energy Future, *Report to NOAA-NMFS Hydropower Coordination Office*, University of Alaska Fairbanks.

Cogley, J.G., 1999. Effective sample size for glacier mass balance, *Geografiska Annaler: Series A, Physical Geography*, **81**, 497–507.

Cogley, J.G., A.A. Arendt, A. Bauder, R.J. Braithwaite, R. Hock, P. Jansson, G. Kaser, M. Möller, L. Nicholson, L.A. Rasmussen and M. Zemp, 2011. Glossary of Glacier Mass Balance and Related Terms, *IHP-VII Technical Documents in Hydrology No. XX, IACS Contribution No. 2*, UNESCO-IHP.

Cox, L. and R. March, 2004. Comparison of geodetic and glaciological mass balance, Gulkana Glacier, Alaska, USA, *Journal of Glaciology*, **50**(170), 363–370.

Daly, C., W. P Gibson, G. H Taylor, G.L. Johnson and P. Pasteris, 2002. A knowledge-based approach to the statistical mapping of climate, *Climate Research*, **22**(2), 99–113.

Daly, C., R. Neilson and D. Philips, 1994. A statistical-topographic model for mapping climatological precipitation over mountainous terrain, *Journal of Applied Meteorology*, **33**, 140–158.

Dyurgerov, M. and M. Meier, 2000. Twentieth century climate change: evidence from small glaciers, *Proceedings of the National Academy of Sciences of the United States of America*, **97**(4), 1406–1411.

Echelmeyer, K., W. Harrison, C. Larsen, J. Sapiano, J. Mitchell, J. DeMallie, B. Rabus, G. Aðalgeirsdóttir and L. Sombardier, 1996. Airborne surface profiling of glaciers: a case-study in Alaska, *Journal of Glaciology*, **42**(142), 538–547.

Gardner, A., G. Moholdt, J.G. Cogley, B. Wouters, A. Arendt, J. Wahr, E. Berthier, R. Hock, W.T. Pfeffer, G. Kaser, S. Ligtenberg, T. Bolch, M. Sharp, J.O. Hagen, M. van den Broeke and F. Paul, 2013. A reconciled estimate of glacier contributions to sea level rise: 2003 to 2009, *Science*, **340**(6134), 852–857.

Gesch, D.B., 2007. Digital Elevation Model Technologies and Applications: The DEM Users Manual, 2nd Edition, Asprs Publications.

Gesch, Dean, Michael Oimoen, Susan Greenlee, Charles Nelson, Michael Steuck and Dean Tyler, 2002. The National Elevation Dataset, *Journal of the American Society for Photogrammetry and Remote Sensing*, **68**(1).

Goodwin, K., M.G. Loso and M. Braun, 2012. Glacial transport of human waste and survival of fecal bacteria on Mt. McKinley's Kahiltna Glacier, Denali National Park, Alaska, *Arctic, Antarctic, and Alpine Research*, **44**(4), 432–445.

Gusmeroli, A., A. Arendt, D. Atwood, B. Kampes, M. Sanford and J. Young, 2013. Variable penetration depth of interferometric synthetic aperture radar signals on Alaska glaciers: a cold surface layer hypothesis, *Annals of Glaciology*, **54**(64), 218–223.

Hinzman, L., N. Bettez, W. Bolton, F. Chapin, M. Dyurgerov, C. Fastie, B. Griffith, R. Hollister, A. Hope, H. Huntington, A. Jensen, G. Jia, T. Jorgenson, D. Kane, D. Klein, G. Kofinas, A. Lynch, A. Lloyd, A. McGuire, F. Nelson, W. Oechel, T. Osterkamp, C. Racine, V. Romanovsky, R. Stone, D. Stow, M. Sturm, C. Tweedie, G. Vourlitis, M. Walker, D. Walker, P. Webber, J. Welker, K. Winker and K. Yoshikawa, 2005. Evidence and implications of recent climate change in northern Alaska and other Arctic regions, *Climatic Change*, **72**, 251–298.

Hock, R., 1999. A distributed temperature-index ice- and snowmelt model including potential direct solar radiation, *Journal of Glaciology*, **45**(149), 101–111.

Hock, R., 2005. Glacier melt: a review of processes and their modelling, *Progress in Physical Geography*, **29**(3), 362–391.

Hood, E. and L. Berner, 2009. The effect of changing glacial coverage on the physical and biogeochemical properties of coastal streams in southeastern Alaska, *Journal of Geophysical Research*, **114**(13), G03001.

Hood, E., J. Fellman, R.G.M. Spencer, P.J. Hernes, R. Edwards, D. D'Amore and D. Scott, 2009. Glaciers as a source of ancient and labile organic matter to the marine environment, *Nature*, **462**(7276), 1044–1048.

Hood, E. and D. Scott, 2008. Riverine organic matter and nutrients in Southeast Alaska affected by glacial coverage, *Nature Geoscience*, **1**(9), 583–587.

Huss, M., 2013. Density assumptions for converting geodetic glacier volume change to mass change, *The Cryosphere*, **7**(3), 877–887.

Jacob, T., J. Wahr, W.T. Pfeffer and S. Swenson, 2012. Recent contributions of glaciers and ice caps to sea level rise, *Nature*, **482**(7386), 514–8.

Johnson, A., C. Larsen, N. Murphy, A. Arendt and S.L. Zirnheld, 2013. Mass balance in the Glacier Bay area of Alaska, USA and and British Columbia, Canada, 1995-2011 using airborne laser altimetry, *Journal of Glaciology*, **59**(216), 632–648.

Kalnay, E., M. Kanamitsu, R. Kistler, W. Collins, D. Deaven, L. Gandin and M. Iredell, 1996. The NCEP/NCAR 40-year reanalysis project, *Bulletin of the American Meteorological Society*, **77**(3), 437–471.

Kaser, G., J. G. Cogley, M. B. Dyurgerov, M. F. Meier and A. Ohmura, 2006. Mass balance of glaciers and ice caps: consensus estimates for 1961-2004, *Geophysical Research Letters*, **33**(19), L19501.

Kayastha, R.B., Y. Takeuchi, M. Nakawo and Y. Ageta, 2000. Practical prediction of ice melting beneath various thickness of debris cover on Khumbu Glacier, Nepal, using a positive degree-day factor, *IAHS PUBLICATION*, 71–82.

King, M.A., 2009. The GPS contribution to the error budget of surface elevations derived from airborne LIDAR, *IEEE Transactions on Geoscience and Remote Sensing*, **47**(3), 874–883.

Larsen, C., R. Motyka, A. Arendt, K. Echelmeyer and P. Geissler, 2007. Glacier changes in Southeast Alaska and northwest British Columbia and contribution to sea level rise, *Journal of Geophysical Research*, **112**(1), F01007.

Larsen, C., R. Motyka, J. Freymuller, K. Echelmeyer and E. Ivins, 2005. Rapid viscoelastic uplift in Southeast Alaska caused by post-Little Ice Age glacial retreat, *Earth and Planetary Science Letters*, **237**, 548–560.

Luthcke, S., A. Arendt, D. Rowlands, C. Larsen and J. McCarthy, 2008. Recent glacier mass changes in the Gulf of Alaska region from GRACE mascon solutions, *Journal of Glaciology*, **54**(188), 767–777.

Luthcke, S., T. Sabaka, B. Loomis, A. Arendt, J. McCarthy and J. Camp, 2013. Antarctica, Greenland and Gulf of Alaska land-ice evolution from an iterated GRACE global mascon solution, *Journal of Glaciology*, **59**(216), 613–631.

MacCluskie, M., K. Oakley, T. McDonald and D. Wilder, 2005. Central Alaska Network Vital Signs Monitoring Plan, *Technical report*, National Park Service.

Mantey, K., 2012. IFSAR Quality Assurance Report: Fugro Earth Data, Inc. Cells D, E, and F in Alaska, *Technical report*, Dewberry.

Mattson, L.E., J.S. Gardner and G.J. Young, 1993. Ablation on debris covered glaciers: an example from the Rakhiot Glacier, Punjab, Himalaya, *IAHS Publications-Publications of the International Association of Hydrological Sciences*, **218**, 289–296.

Mayo, L., 2001. Manual for Monitoring Glaciers at Denali National Park, Alaska, Using the Index Site Method, *Technical report*, National Park Service.

Meier, M.F., M.B. Dyurgerov, U.K. Rick, S. O'Neel, W.T. Pfeffer, R.S. Anderson, S.P. Anderson and A.F. Glazovsky, 2007. Glaciers dominate eustatic sea-level rise in the 21st century, *Science*, **317**(5841), 198–199.

Motyka, R.J., M. Fahnestock and M. Truffer, 2010. Volume change of Jakobshavn Isbrae, West Greenland: 1985–1997–2007, *Journal of Glaciology*, **56**(198), 635–646.

Neal, E., E. Hood and K. Smikrud, 2010. Contribution of glacier runoff to freshwater discharge into Gulf of Alaska, *Geophyiscal Research Letters*, **37**(6), L06404.

Oerlemans, J., 2000. Analysis of a 3 year meteorological record from the ablation zone of Morteratschgletscher, Switzerland: energy and mass balance, *Journal of Glaciology*, **46**(155), 571–579.

Oerlemans, J., 2010. The Microclimate of Valley Glaciers, Igitur, Utrecht Publishing & Archiving Services.

Ohmura, A., 2001. Physical basis for the temperature-based melt-index method, *Journal of Applied Meteorology*, **40**(4), 753–761.

Ohmura, A., P. Kasser and M. Funk, 1992. Climate at the equilibrium line of glaciers, *Journal of Glaciology*, **38**(130), 397–411.

Østrem, G., 1959. Ice melting under a thin layer of moraine, and the existence of ice cores in moraine ridges, *Geografiska Annaler*, **41**(4), 228–230.

Østrem, G. and M. Brugman, 1991. Glacier Mass-Balance Measurements, *Technical report*, National Hydrology Research Institute.

Overland, J.E., M. Wang and N.A. Bond, 2002. Recent temperature changes in the western Arctic during spring, *Journal of Climate*, **15**(13), 1702–1716.

Pfeffer, W.T., A. Arendt, A. Bliss, T. Bolch, J.G. Cogley, A.S. Gardner, J.O. Hagen, R. Hock, G. Kaser, C. Kienholz, E.S. Miles, G. Moholdt, N. Moelg, F. Paul, V. Radić, P. Rastner, B.H. Raup, J. Rich, M.J. Sharp and the Randolph Consortium, In Press. The Randolph Glacier Inventory: a globally complete inventory of glaciers, *Journal of Glaciology*.

Pritchard, H., S. Luthcke and A. Fleming, 2010. Understanding ice-sheet mass balance: progress in satellite altimetry and gravimetry, *Journal of Glaciology*, **56**(200), 1151–1161.

Radić, V., A. Bliss, A.C. Beedlow, R. Hock, E. Miles and J.G. Cogley, 2013. Regional and global projections of twenty-first century glacier mass changes in response to climate scenarios from global climate models, *Climate Dynamics*, **1**, 1–22.

Radić, V. and R. Hock, 2011. Regionally differentiated contribution of mountain glaciers and ice caps to future sea-level rise, *Nature Geoscience*, **4**(2), 91–94.

Rasmussen, L. and H. Conway, 2004. Climate and glacier variability in western North America, *Journal of Climate*, **17**, 1804–1815.

Rasmussen, L.A., H. Conway, R.M. Krimmel and R. Hock, 2011. Surface mass balance, thinning and iceberg production, Columbia Glacier, Alaska, 1948–2007, *Journal of Glaciology*, **57**(203), 431–440.

Rignot, E., A. Rivera and G. Casassa, 2003. Contribution of the Patagonia Icefields of South America to sea level rise, *Science*, **302**(5644), 434–437.

Rolstad, C., T. Haug and B. Denby, 2009. Spatially integrated geodetic glacier mass balance and its uncertainty based on geostatistical analysis: application to the western Svartisen ice cap, Norway, *Journal of Glaciology*, **55**(192), 666–680.

Royer, T.C., 1981. Baroclinic transport in the Gulf of Alaska. Part II. A fresh water driven coastal current, *Journal of Marine Research*, **39**, 251–266.

Sapiano, J.J., W.D. Harrison and K.A. Echelmeyer, 1998. Elevation, volume and terminus changes of nine glaciers in North America, *Journal of Glaciology*, **44**(146), 119–135.

Sasgen, I., V. Klemann and Z. Martinec, 2012. Towards the inversion of GRACE gravity fields for present-day ice-mass changes and glacial-isostatic adjustment in North America and Greenland, *Journal of Geodynamics*, **59**, 49–63.

Sato, T., S. Miura, W. Sun, T. Sugano, J.T. Freymueller, C.F. Larsen, Y. Ohta, H. Fujimoto, D. Inazu and R.J. Motyka, 2012. Gravity and uplift rates observed in Southeast Alaska and their comparison with GIA model predictions, *Journal of Geophysical Research: Solid Earth (1978–2012)*, **117**(B1).

Schubert, C., R.S. Williams and J.G. Ferrigno, 1998. Satellite Image Atlas of Glaciers of the World, U.S. Government Printing Office, U.S. Geological Survey.

Serreze, M. C., J. E. Walsh, F. S. Chapin, T. Osterkamp, M. Dyurgerov, V. Romanovsky, W. C. Oechel, J. Morison, T. Zhang and R. G. Barry, 2000. Observational evidence of recent change in the Northern High-latitude environment, *Climatic Change*, **46**, 159–207.

Simpson, J.J., G.L. Hufford, C. Daly, J.S. Berg and M.D. Fleming, 2005. Comparing maps of mean monthly surface temperature and precipitation for Alaska and adjacent areas of Canada produced by two different methods, *Arctic*, **58**, 137–161.

Stafford, J.M., G. Wendler and J. Curtis, 2000. Temperature and precipitation of Alaska: 50 year trend analysis, *Theoretical and Applied Climatology*, **67**, 33–44.

Tamisiea, M., E. Leuliette, J. Davis and J. Mitrovica, 2005. Constraining hydrological and cryospheric mass flux in southeastern Alaska using space-based gravity measurements, *Geophysical Research Letters*, **32**(20), L20501.

Thibert, E., R. Blanc, C. Vincent and N. Eckert, 2008. Glaciological and volumetric mass-balance measurements: error analysis over 51 years for Glacier de Sarennes, French Alps, *Journal of Glaciology*, **54**(186), 522–532.

Trüssel, B., R.J. Motyka, M. Truffer and C.F. Larsen, 2013. Rapid thinning of lake-calving Yakutat Glacier and the collapse of the Yakutat Icefield, southeast Alaska, USA, *Journal of Glaciology*, **59**(213), 149–161.

Van Beusekom, A., S. O'Neel, R. March, L. Sass and L. Cox, 2010. Re-analysis of Alaskan Benchmark Glacier Mass-balance Data Using the Index Method, *Scientific investigations report*, U.S. Geological Survey.

VanLooy, J., R. Forster and A. Ford, 2006. Accelerating thinning of Kenai Peninsula glaciers, Alaska, *Geophysical Research Letters*, **33**(21), L21307.

Wu, X., M. Heflin, H. Schotman, B. Vermeersen, D. Dong, R. Gross, E. Ivins, A. Moore and S. Owen, 2010. Simultaneous estimation of global present-day water transport and glacial isostatic adjustment, *Nature Geoscience*, **3**(9), 642–646.

Young, J., A. Arendt and J. Hulth, 2011. Notes on AWS measurements on the Kahiltna Glacier, Central Alaska Range, and a Simple Floating Temperature Stand Design, *Technical report*, International Arctic Science Committee.

Zemp, M., M. Hoelzle and W. Haeberli, 2009. Six decades of glacier mass-balance observations: a review of the worldwide monitoring network, *Annals of Glaciology*, **50**(50), 101–111.

Appendix A

In order to expand on existing observation programs, both to fill spatial gaps and to measure additional variables, two seasons of field campaigns were carried out on the Kahiltna Glacier in 2010 and 2011. These campaigns were motivated primarily by a need for in-situ measurements that would serve as input and calibration for the mass balance model simulations.

A.1 Mass balances

Field trips were conducted in both early spring and late summer, in order to capture end-of-winter conditions and the full duration of the melt season. Mass balance stakes were installed along a centerline, between 808 m and 1409 m elevation in 2010 (9 stakes, with two at the same elevation but in different across-glacier locations; Fig. A.1a, Table A.1) and between 790 m and 2004 m in 2011 (11 stakes, with three at the same elevation and location; Fig. A.1b, Table A.2). Unfortunately, attempts to collect data from stakes at 2317 m and 3231 m were not successful. The former location did not have an obvious summer surface from which to estimate winter balance, and snowfall throughout the summer made summer melt difficult to quantify; the latter stake was never recovered.

Snow depth and density measurements were obtained by standard methods using graduated avalanche probes and density sampling kits for snow pits (containing a 0.5 L volume sampler, snow cutting tools and spring scale with dry bag). Figure A.2 shows the locations of observations made in each 2010 and 2011. Tables A.3 and A.4 provide snow depth and density measurements at the pit locations, and tables A.5 and A.6 provide all snow depth measurements and associated winter balances.

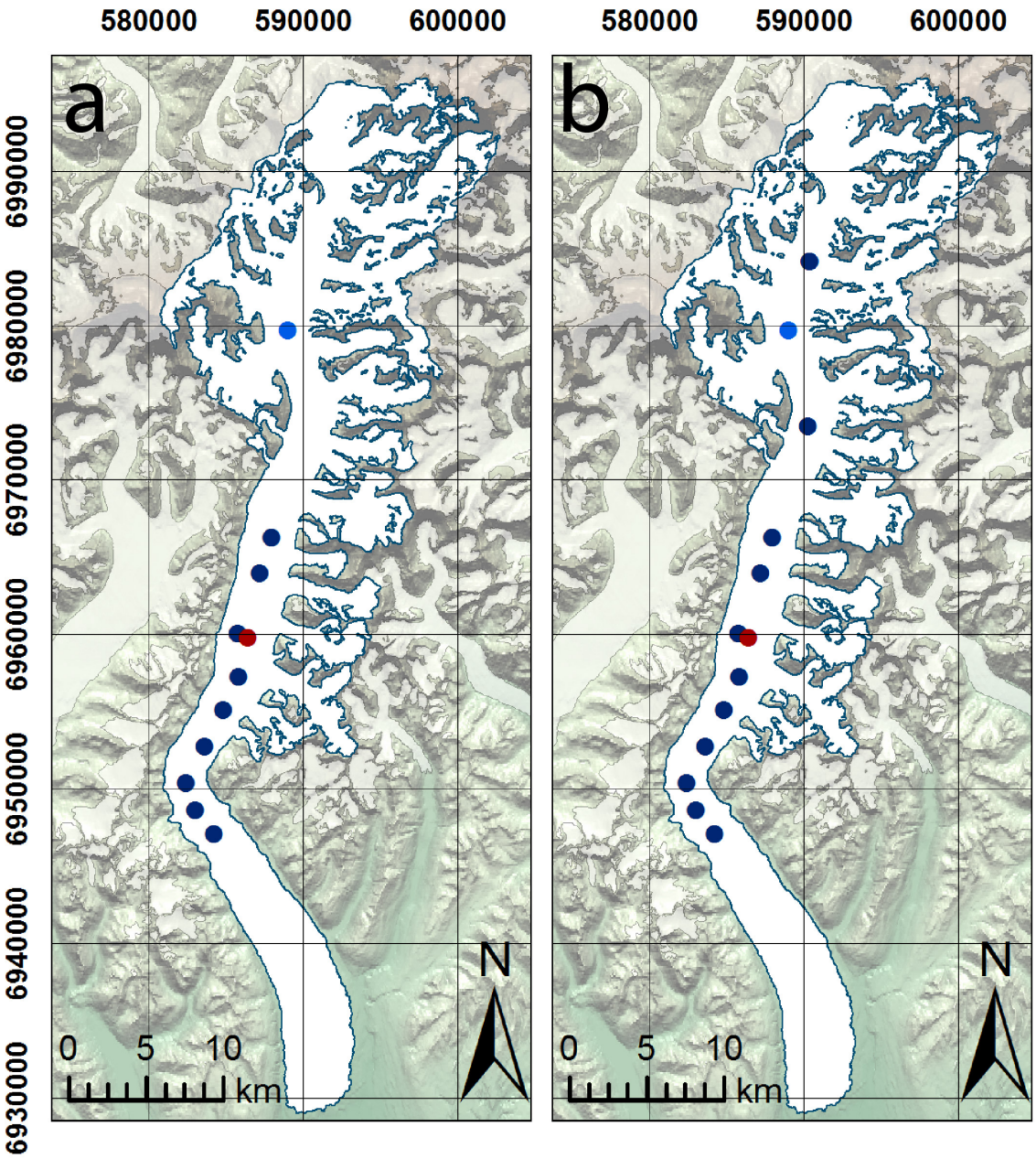

Figure A.1. Location of 2010 and 2011 mass balance and on-glacier weather station measurements. a) Instruments installed in 2010, between 808 m and 1409 m. b) Instruments installed in 2011, between 790 m and 2004 m. Ablation stakes are shown in dark blue, the NPS index site stake is in light blue, and the location of our automated weather station is in red.

Table A.1. Summary of 2010 point mass balance measurements. Note that stake elevations and locations are given as the starting position of the first listed date (end positions and velocities are given in Table A.7), and that start dates for b_w measurements are estimated from air temperature records. Note also that while b_w is a best estimate of the balance for the full winter season, b_s values represent balances measured exactly between the dates listed, and therefore may not have captured the full summer melt season.

Stake name	Elevation (m)	UTM zone 5V easting (m)	UTM zone 5V northing (m)	b_w (m w.e.)	b_s (m w.e.)	Start date	End date
KT1	1409.3	587977.2	6966285.0	0.60		10/27/09	04/30/10
					-2.08	04/30/10	08/26/10
KS10	1238.8	585754.9	6960046.2	0.55		10/27/09	05/04/10
					-2.66	05/04/10	08/26/10
KT2	1235.5	586444.0	6959787.9	0.55		10/27/09	05/04/10
					-1.95	05/04/10	08/26/10
KS2	1163.8	585829.5	6957249.2	0.65		10/27/09	05/03/10
					-2.17	05/03/10	08/26/10
KT3	1099.5	584823.3	6955102.5	0.63		10/27/09	05/01/10
					-2.28	05/01/10	08/26/10
KS3	1007.4	583631.5	6952743.5	0.64		10/27/09	05/03/10
					-2.73	05/03/10	08/26/10
KT4	951	582440.2	6950375.1	0.48		10/27/09	05/02/10
					-3.29	05/02/10	08/26/10
KS4	862	583042.7	6948637.9	0.56		10/27/09	05/02/10
					-3.02	05/02/10	08/26/10
KT5	808.4	584248.6	6947092.1	0.46		10/27/09	05/02/10
					-3.15	05/02/10	08/26/10

Table A.2. Summary of 2011 point mass balance measurements. Note that stake elevations and locations are given as the starting position of the first listed date (end positions and velocities are given in Table A.7), and that start dates for b_w measurements are estimated from air temperature records. Note also that while b_w is a best estimate of the balance for the full winter season, b_s values represent balances measured exactly between the dates listed, and therefore may not have captured the full summer melt season.

Stake name	Elevation (m)	UTM zone 5V easting (m)	UTM zone 5V northing (m)	b_w (m w.e.)	b_s (m w.e.)	Start date	End date
KH3	2004.5	590380.5	6984170.2		-1.04	06/06/11	08/15/11
KH4	1649.9	590271.5	6973523.8		-1.85	06/06/11	08/15/11
KT1	1396.3	587952.6	6966233.3	0.48		10/06/10	04/25/11
					-3.21	04/25/11	09/14/11
KS1	1310.3	587196.7	6963950.3	0.56		10/06/10	04/25/11
					-3.04	04/25/11	09/14/11
KT2	1211.6	586401.3	6959567.6	0.63		10/06/10	04/30/11
					-3.88	04/30/11	09/14/11
SR50	1211.6	586401.3	6959567.6	0.61		10/06/10	04/26/11
					-3.20	04/26/11	09/14/11
draw	1211.6	586401.3	6959567.6	0.61		10/06/10	05/01/11
					-2.91	05/01/11	09/14/11
KT3	1066.9	584580.4	6955095.9	0.54		10/06/10	04/27/11
					-3.43	04/27/11	09/14/11
KS3	994.7	583602.7	6952719.1	0.62		10/06/10	04/29/11
					-3.78	04/29/11	09/14/11
KT4	897.3	582460.1	6950330.4	0.62		10/06/10	04/28/11
					-4.09	04/28/11	09/14/11
KT5	790.8	584284.5	6947053.0	0.53		10/06/10	04/28/11
					-4.23	04/28/11	09/14/11

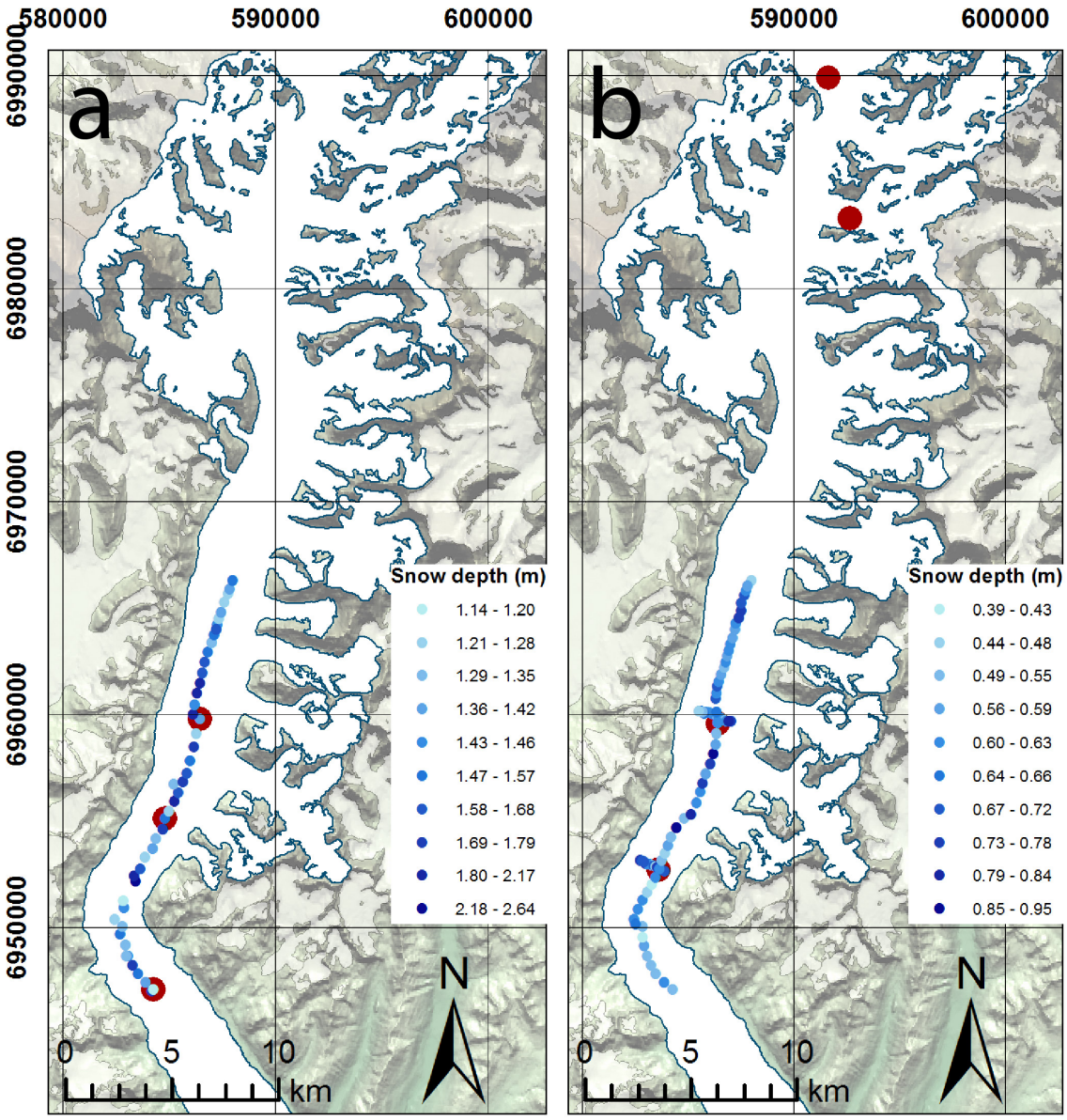

Figure A.2. Location of 2010 and 2011 snow depth and density measurements. a) Elevations spanned in 2010 were between 808 m and 1409 m. b) Elevations spanned in 2011 were between 790 m and 2004 m. Snow pit locations are shown in red, although data from the two uppermost 2011 pits were not used for the winter balance calculations due to the late timing of the measurements. Snow depth is shown according to scale in blue.

Table A.3. Snow depth and density measurements from spring 2010 snow pits. Measurements were made at KT2 on May 5, at KT3 on May 1, and at KT5 on May 2.

KT2		KT3		KT5	
Mean depth (cm)	Mean density (kg m^{-3})	Mean depth (cm)	Mean density (kg m^{-3})	Mean depth (cm)	Mean density (kg m^{-3})
9.5	359.2	11.5	305.2	9.5	379.7
28.5	359.2	33.0	292.5	28.5	328.4
47.5	410.5	52.5	369.5	48.5	315.7
66.5	400.3	70.5	447.4	67.5	435.9
85.5	390.0	88.5	379.7	87.0	363.4
104.5	400.3	107.5	390.0	106	536.3
117.0	425.8	121.0	370.5	116.5	468.0

Table A.4. Snow depth and density measurements from spring 2011 snow pits. Measurements were made at KT2 on April 30, and at KS3 on April 29.

KT2		KS3	
Mean depth (cm)	Mean density (kg m^{-3})	Mean depth (cm)	Mean density (kg m^{-3})
11.0	189.7	10.0	282.8
31.5	244.3	30.0	263.3
51.0	354.9	50.0	331.5
70.5	359.2	70.0	370.5
90.5	293.4	90.0	390.0
110.5	338.7	110.0	321.8
130.0	481.7	130.0	399.8
150.0	462.2	150.0	399.8
		167.5	507.0

Table A.5: Snow depth measurements collected between April 30 and May 4, 2010, and associated winter balance estimate.

Elevation (m)	UTM zone 5V Easting (m)	UTM zone 5V Northing (m)	Depth 1 (m)	Depth 2 (m)	Depth 3 (m)	Depth 4 (m)	Mean depth (m)	b_w (m w.e.)
792	584176.0	6946997.1	1.66	1.72	1.72	1.73	1.71	0.69
803	583888.5	6947413.4	1.38	1.38	1.38	1.42	1.39	0.54
821	583539.8	6947816.9	1.52	1.57	1.46	1.59	1.54	0.61
831	583252.7	6948222.1	1.89	1.89	1.62	1.67	1.77	0.72
843	582712.6	6948498.3	1.14	1.13	1.14		1.14	0.43
847	583042.3	6948640.3	1.43				1.43	0.56
847	583557.5	6948943.1	1.69	1.69	1.70		1.69	0.68
852	583001.3	6948639.3	1.35	1.22	1.35	1.33	1.31	0.51
864	582926.4	6949172.4	1.28	1.38	1.38	1.21	1.31	0.51
879	582688.2	6949679.1	1.51	1.56	1.62		1.56	0.62
880	582786.8	6950038.2	1.36	1.37	1.33	1.35	1.35	0.52
913	582882.5	6950921.2	1.35	1.48	1.46	1.44	1.43	0.56
932	582843.7	6951243.4	1.13	1.17	1.08	1.18	1.14	0.43
981	583414.4	6952171.7	2.64				2.64	1.18
985	583357.3	6952404.3	1.97	1.97	1.97	1.97	1.97	0.82
995	583630.3	6952745.6	1.62	1.48	1.64	1.65	1.60	0.64
1010	583862.3	6953286.5	1.25	1.26	1.37	1.19	1.27	0.49

Elevation (m)	UTM zone 5V Easting (m)	UTM zone 5V Northing (m)	Depth 1 (m)	Depth 2 (m)	Depth 3 (m)	Depth 4 (m)	Mean depth (m)	b_w (m w.e.)
1021	584210.2	6953696.6	1.34	1.38	1.48	1.45	1.41	0.55
1041	584367.0	6954168.8	1.31				1.31	0.51
1057	584709.3	6954589.9	1.78	1.76	1.64	1.66	1.71	0.69
1070	585324.3	6954750.7	1.55	1.69	1.48		1.57	0.63
1072	585236.0	6954804.1	1.64	1.63	1.55		1.61	0.64
1074	585152.7	6954857.7	1.34	1.34	1.34		1.34	0.52
1074	584731.1	6955136.6	1.20	1.42	1.42	1.25	1.32	0.51
1074	584647.8	6955190.2	1.43	1.56	1.32		1.44	0.56
1074	584611.5	6955211.6	1.44	1.30	1.17	1.25	1.29	0.50
1075	584585.6	6955222.1	1.45	1.44	1.37		1.42	0.55
1075	584674.0	6955168.6	1.25	1.17	1.03	1.19	1.16	0.44
1077	584554.4	6955243.6	1.43	1.42	1.25		1.37	0.53
1079	585069.4	6954911.3	1.33	1.24	1.58	1.42	1.39	0.54
1080	584986.2	6954964.9	1.19	1.18	1.15		1.17	0.45
1080	584818.8	6955105.5	1.72	1.50	1.70	1.37	1.57	0.63
1081	584908.1	6955018.6	1.77	1.81	1.68		1.75	0.71
1090	585004.2	6955455.8	1.22	1.27	1.30	1.16	1.24	0.47
1108	585238.4	6955896.5	2.29	2.13	1.95	2.16	2.13	0.90
1124	585446.9	6956336.6	1.60	1.60	1.66	1.67	1.63	0.65
1129	585206.9	6956720.5	1.35				1.35	0.52
1138	585649.2	6956821.1	1.73	1.72	1.72	1.83	1.75	0.71

Elevation (m)	UTM zone 5V Easting (m)	UTM zone 5V Northing (m)	Depth 1 (m)	Depth 2 (m)	Depth 3 (m)	Depth 4 (m)	Mean depth (m)	b_w (m w.e.)
1152	585991.5	6957810.9	1.54	1.56	1.56	1.59	1.56	0.62
1169	586147.7	6958483.8	1.72	1.74	1.83	1.87	1.79	0.73
1180	586274.4	6959111.3	1.24	1.26	1.23	1.23	1.24	0.47
1213	586088.2	6959975.8	1.34	1.25	1.29	1.20	1.27	0.49
1213	585990.6	6959995.5	1.28	1.26	1.28	1.33	1.29	0.50
1214	586372.2	6959860.6	1.47	1.55	1.57	1.56	1.54	0.61
1214	586186.1	6959944.9	1.18	1.17	1.29	1.27	1.23	0.47
1214	586440.7	6959784.4	1.33	1.49	1.41	1.37	1.40	0.55
1215	586279.2	6959902.8	1.62	1.67	1.73	1.49	1.63	0.65
1215	585887.7	6960026.3	1.28	1.29	1.33	1.34	1.31	0.51
1216	585887.7	6960026.3	1.07	1.12	1.09	1.09	1.09	0.41
1217	586107.5	6960020.9	2.00				2.00	0.83
1217	586543.4	6959764.8	1.59	1.62	1.64	1.58	1.61	0.64
1219	585790.1	6960046.0	1.42	1.28	1.31	1.48	1.37	0.53
1222	586641.0	6959745.1	1.53	1.47	1.47	1.52	1.50	0.59
1223	585687.7	6960054.5	1.33	1.27	1.33	1.27	1.30	0.50
1223	585590.1	6960074.2	1.33	1.34	1.80	2.00	1.62	0.65
1224	586738.6	6959725.4	1.42	1.52	1.46	1.53	1.48	0.58
1225	586836.2	6959705.6	1.56	1.63	1.57	1.37	1.53	0.61
1225	586938.6	6959697.2	1.58	1.60	1.66	1.58	1.61	0.64
1228	587036.2	6959677.5	1.38	1.42	1.34	1.28	1.36	0.53

Elevation (m)	UTM zone 5V Easting (m)	UTM zone 5V Northing (m)	Depth 1 (m)	Depth 2 (m)	Depth 3 (m)	Depth 4 (m)	Mean depth (m)	b_w (m w.e.)
1235	586203.3	6960458.1	1.46				1.46	0.57
1255	586307.3	6960973.5	2.17				2.17	0.92
1267	586437.3	6961467.4	2.08				2.08	0.88
1278	586567.3	6961961.2	1.60				1.60	0.64
1286	586682.2	6962443.6	1.68				1.68	0.68
1299	586817.8	6962915.3	1.52				1.52	0.60
1306	586979.1	6963376.5	1.31				1.31	0.51
1310	587102.6	6963725.3	1.52				1.52	0.60
1322	587253.4	6964197.5	1.45				1.45	0.57
1329	587331.7	6964511.7	1.28				1.28	0.49
1336	587441.3	6964804.4	1.42				1.42	0.55
1352	587592.5	6965254.3	1.22				1.22	0.47
1374	587750.3	6965648.6	1.26				1.26	0.48
1385	587840.9	6965885.1	1.40				1.40	0.55
	587202.6	6963995.5	1.63				1.63	0.65
	585822.1	6957249.2	1.37	1.96	1.83	1.37	1.63	0.65
	587972.9	6966289.9	1.52				1.52	0.60
	582440.2	6950375.1	1.20	1.18	1.58	1.16	1.26	0.49
	584250.6	6947088.2	1.28	1.17	1.26	1.08	1.20	0.46

Table A.6: Snow depth measurements collected between April 25 and May 1, 2011, and associated winter balance estimate.

Elevation (m)	UTM zone 5V Easting (m)	UTM zone 5V Northing (m)	Depth 1 (m)	Depth 2 (m)	Depth 3 (m)	Depth 4 (m)	Mean depth (m)	b_w (m w.e.)
802	583857.5	6947423.7	1.59	1.77	1.71		1.69	0.60
818	583457.9	6947814.9	1.50	1.89	1.39		1.59	0.55
829	583227.1	6948221.4	1.54	1.50	1.45		1.50	0.51
838	583036.9	6948651.3	1.74	1.59	1.48		1.60	0.55
855	582907.0	6949127.3	1.75	1.44	1.76		1.65	0.58
867	582850.9	6949527.2	1.17	1.34	1.35		1.29	0.41
875	582842.9	6950050.8	1.61	1.49	1.53		1.54	0.53
890	582497.0	6950153.6	1.82	1.85	1.80		1.82	0.66
909	582607.4	6950858.5	1.74	1.74	1.72		1.73	0.62
933	582837.7	6951276.7	1.74	1.72	1.76		1.74	0.62
957	583053.4	6951661.1	1.41	1.41	1.41		1.41	0.47
974	583179.5	6952957.1	1.76	1.85	1.88		1.83	0.66
976	583285.3	6952012.4	1.31	1.21	1.16		1.23	0.39
983	583267.3	6952925.9	1.40	1.19	1.35		1.31	0.43
984	582983.7	6953007.9	2.30	2.35	2.31		2.32	0.92
985	582718.8	6953157.3	1.95	1.99	2.05		2.00	0.75
986	582817.4	6953104.1	1.89	1.91	1.89		1.90	0.70

Elevation (m)	UTM zone 5V Easting (m)	UTM zone 5V Northing (m)	Depth 1 (m)	Depth 2 (m)	Depth 3 (m)	Depth 4 (m)	Mean depth (m)	b_w (m w.e.)
986	583076.6	6952976.8	1.73	1.66	1.73		1.71	0.60
987	583466.2	6952351.4	1.76	1.74	1.75		1.75	0.62
988	582890.2	6953061.3	1.89	1.85	1.90		1.88	0.69
991	583370.8	6952883.9	2.00	1.79	1.92		1.90	0.70
991	583909.7	6952630.1	1.90	1.85	1.90		1.88	0.69
991	583458.9	6952841.6	1.45	1.29	1.61		1.45	0.48
991	583629.7	6952767.9	1.76	1.77	1.76		1.76	0.63
992	583547.0	6952799.2	2.02	1.97	2.05		2.01	0.76
992	583723.2	6952714.5	1.89	1.97	1.94		1.93	0.72
992	583816.5	6952672.3	1.93	1.83	1.91		1.89	0.69
995	583630.3	6952745.6	1.73	1.73	1.75		1.74	0.62
1006	583733.2	6953127.2	1.52	1.71	1.30		1.51	0.51
1017	583898.1	6953488.0	1.27	1.40	1.46		1.38	0.45
1023	584047.9	6953837.4	1.68	1.70	1.58		1.65	0.58
1034	584191.1	6954242.3	1.54	1.39	1.54		1.49	0.50
1052	584425.5	6954683.0	2.34	2.29	2.44		2.36	0.95
1079	584818.8	6955105.5	1.58	1.56	1.56		1.57	0.54
1090	585136.7	6955280.8	2.11	2.21	2.19		2.17	0.84
1113	585392.9	6955855.9	1.86	1.78	1.59		1.74	0.62
1125	585564.5	6956339.6	1.74	1.75	1.73		1.74	0.62
1133	585696.9	6956755.5	2.06	1.98	2.01		2.02	0.76

Elevation (m)	UTM zone 5V Easting (m)	UTM zone 5V Northing (m)	Depth 1 (m)	Depth 2 (m)	Depth 3 (m)	Depth 4 (m)	Mean depth (m)	b_w (m w.e.)
1144	585813.0	6957204.4	1.61	1.62	1.74		1.66	0.58
1154	586041.3	6957667.3	2.20	2.20	1.74		2.05	0.77
1162	586177.5	6958127.9	2.42	2.27	2.18		2.29	0.91
1169	586309.1	6958566.0	1.58	1.71	1.75		1.68	0.59
1185	586341.4	6959090.7	1.75	1.40	1.53		1.56	0.53
1208	586404.2	6959616.2	1.73	1.73	1.78		1.75	0.62
1214	586194.9	6960000.9	1.67	1.75	1.55		1.66	0.58
1215	586282.8	6959958.6	2.20	2.20	1.80		2.07	0.79
1216	586106.6	6960054.3	1.72	1.71	1.69		1.71	0.60
1216	586371.1	6959905.2	1.50	1.48	1.60		1.53	0.52
1217	585910.9	6960116.0	1.31	1.30	1.58		1.40	0.46
1218	586013.5	6960096.4	1.75	1.74	1.80		1.76	0.63
1218	586547.3	6959809.5	1.72	1.75	1.77		1.75	0.62
1219	586459.0	6959862.9	1.64	1.70	1.84		1.73	0.61
1220	585803.4	6960124.4	1.82	1.68	1.81		1.77	0.63
1221	586640.7	6959756.2	1.70	1.72	1.74		1.72	0.61
1221	585759.4	6960045.2	1.82	1.80	1.75	1.76	1.78	0.64
1223	586733.8	6959714.1	1.51	1.50	1.62		1.54	0.53
1223	586329.8	6960115.9	1.79	1.80	1.77		1.79	0.64
1224	585598.6	6960141.3	1.83	1.85	1.80		1.83	0.66
1224	585701.0	6960132.9	1.60	1.61	1.42		1.54	0.53

Elevation (m)	UTM zone 5V Easting (m)	UTM zone 5V Northing (m)	Depth 1 (m)	Depth 2 (m)	Depth 3 (m)	Depth 4 (m)	Mean depth (m)	b_w (m w.e.)
1224	586831.6	6959683.2	1.72	1.73	1.70		1.72	0.61
1225	587031.4	6959666.2	2.05	2.00			2.03	0.76
1226	586933.8	6959685.9	2.10	2.11	2.05		2.09	0.80
1227	585485.7	6960160.7	1.50	1.45	1.38		1.44	0.48
1247	586318.5	6960739.8	1.90	1.80	1.89		1.86	0.68
1253	586352.3	6961008.2	1.70	1.66	1.85		1.74	0.62
1263	586389.8	6961332.4	1.90	1.86	1.89		1.88	0.69
1266	586460.8	6961546.0	1.74	1.74	1.75		1.74	0.62
1275	586574.4	6961883.4	1.60	1.68	1.58		1.62	0.56
1279	586688.4	6962209.6	1.60	1.48	1.55		1.54	0.53
1288	586768.4	6962468.1	1.73	1.74	1.73		1.73	0.62
1294	586847.7	6962748.9	1.60	1.66	1.58		1.61	0.56
1301	586932.5	6963018.6	1.75	1.68	1.70		1.71	0.60
1305	587011.8	6963299.4	1.73	1.72	1.74		1.73	0.61
1309	587091.4	6963569.0	1.68	1.68	1.70		1.69	0.59
1325	587241.4	6964264.1	1.75	1.73	1.70		1.73	0.61
1330	587382.4	6964524.2	2.01	2.07	2.11		2.06	0.78
1337	587501.3	6964850.6	1.96	1.95	1.95		1.95	0.73
1346	587511.6	6965229.8	1.86	1.96	1.95		1.92	0.71
1364	587639.7	6965589.9	1.92	1.81	1.87		1.87	0.68
1379	587730.3	6965826.4	1.74	1.75	1.75		1.75	0.62

Elevation (m)	UTM zone 5V Easting (m)	UTM zone 5V Northing (m)	Depth 1 (m)	Depth 2 (m)	Depth 3 (m)	Depth 4 (m)	Mean depth (m)	b_w (m w.e.)
1385	587801.1	6966040.1	1.71	1.70	1.63		1.68	0.59
1662	590277.3	6973560.0	0.00	0.00	0.00		0.00	0.00
2012	590384.9	6984185.4	0.76	0.78	0.96	0.82	0.83	0.39
2336	591645.1	6989920.0	2.28	2.24			2.26	1.02
3241	593179.8	6995222.2						
1209	586407.7	6959599.7	1.72	1.74	1.75	1.73	1.74	0.62
1224	586408.1	6959604.0	1.78	1.77	1.75		1.77	0.63
2176	592671.2	6983320.2	1.78				1.78	0.85
	587202.6	6963995.5	1.62	1.63	1.62	1.58	1.61	0.56
	585822.1	6957249.2	1.44	1.46	1.45		1.45	0.48
	587972.9	6966289.9	1.43	1.43	1.44		1.43	0.48
	582440.2	6950375.1	1.74	1.77	1.75		1.75	0.63
	584250.6	6947088.2	1.55	1.53	1.56		1.55	0.53

A.2 Air temperature

In order to accurately determine local lapse rates, air temperatures were recorded at five different elevations along the ablation area centerline. Given that snow/ice surfaces generate strong vertical temperature gradients, particularly in the summer (Oerlemans, 2010), floating temperature stands were designed to maintain sensors at a constant height above the glacier surface. In 2010, these stands were built using 1-1/4" inner diameter PVC sleeves fitted over five of the existing 1" outer diameter aluminum mass balance stakes; the former was meant to freely slide down the latter, as the glacier surface lowered (Fig. A.3a). The stands also had square PVC bases, approximately 30 cm x 30 cm, which were intended to act as a footprint that would prevent the stand from melting into the snow or ice. Unfortunately, this initial design did not succeed. Rather than slide down, the PVC sleeves became lodged on the aluminum stakes, either resulting in air temperature readings at significant heights above the glacier surface or, in one case, in the bending and breaking of the aluminum stake under the top-heavy weight of the sensors and stands.

Though the exact reason of the failure is unknown (i.e. whether the stands became lodged simply by mechanical friction or by the formation of melt-refreeze ice between the PVC and aluminum), two adjustments were made to the design when re-installing the sensors in 2011. First, a 1-1/2" PVC sleeve was used in place of the smaller-diameter variety, to allow more room for any thermal expansion of the PVC and aluminum in summer temperatures. Second, the PVC base was completely omitted on the second design, since the base may have contributed too much weight near the bottom of the stand, effectively forcing a point of contact between the PVC and aluminum, thereby pinching itself into place if the stand leaned even slightly.

The improved 2011 design did prevent freezing on the stakes, but without any footprint at all, the bottom of some of the PVC sleeves fell into the ablation stake hole as it widened by melt over the course of the summer. The best floating stand design likely falls somewhere between the two versions; in 2012, a third design, with very simple footprint, was deployed on glaciers on the south side of the Hayes Range as part of another study, with good success (Fig. A.3b).

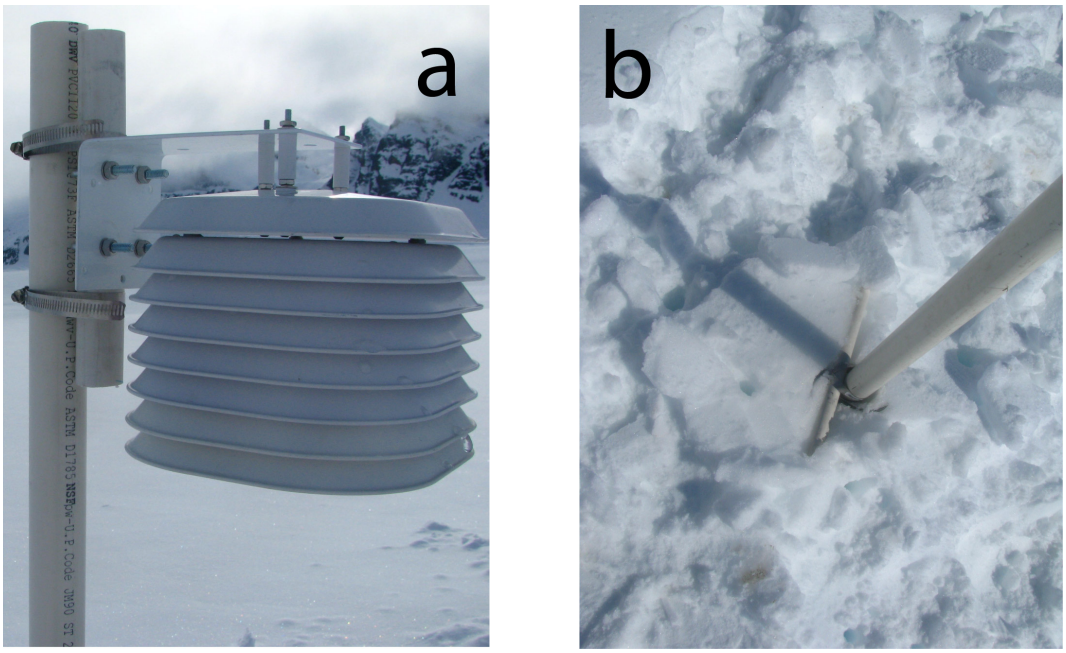

Figure A.3. Floating temperature stand design. a) Top of stand, with sensor and radiation shield attached to PVC sleeve. b) Stand bottom, with simple crosspiece base.

A.2.1 Temperature sensor height correction

Air temperatures recorded in both 2010 and 2011 were corrected from varying heights above the ice surface to a standard 2 m height following an empirically-derived vertical profile determined from the land-terminating Morteratschgletscher in Switzerland (Oerlemans, 2000). This is the only study to fully characterize this logarithmic boundary-layer profile based on actual ground observations. Denoting the height of the sensor above the surface by h, Oerlemans derives the temperature at the standard 2 m height as:

$$T_{2m} = (2/h)^{\mu} * T_h$$

where T_h is the temperature in °C at the height of the sensor, and μ is a constant with a value of 0.126, derived from an empirical analysis of wind and temperature measurements recorded at various sensor heights in summer 1997. Oerlemans points out that this relationship is only useful when the air temperature is above the freezing point, and that otherwise the best one can do is assume that the 2 m temperature is close to the recorded temperature at height h. In other words, $\mu = 0$ if $T_h < 0$ °C.

Applied to our temperature records, using sensor heights that we linearly interpolate between measurement dates, this correction yields an average change of 0.18°C in 2010 and -0.12°C in 2011.

A.3 Velocity data

Velocity measurements were also collected in 2010 and 2011 at the installed ablation stakes (Table A.7). Though these were not explicitly used in this study, measurements are provided for reference.

Table A.7. Velocity measurements collected in 2010 and 2011. Note that easting and northing values are UTM zone 5V, and that error values depend on the accuracy of the GPS unit used to measure stake positions.

Start date	End date	No. of days	Stake name	Start easting (m)	Start northing (m)	End easting (m)	End northing (m)	Velocity (m/day)	Bearing (W = 270°)	Error (m/day)
6/6/11 15:08	8/15/11 12:13	69.88	KH1	593179.8	6995222.2	593172.3	6995226.1	0.12	297.7	0.0052
6/6/11 16:29	8/15/11 11:57	69.81	KH2	591645.1	6989920.0	591656.7	6989899.9	0.33	150.0	0.0045
6/6/11 18:19	8/15/11 10:48	69.69	KH3	590384.9	6984185.4	590376.1	6984155.0	0.45	196.2	0.0045
6/6/11 19:21	8/15/11 13:14	69.75	KH4	590277.3	6973560.0	590265.6	6973487.5	1.05	189.1	0.0045
6/6/11 17:54	9/14/11 12:13	99.76	KT1	587943.7	6966242.6	587928.0	6966181.5	0.63	194.4	0.0032
5/4/10 11:03	9/14/11 13:29	498.10	KT2	586444.0	6959787.9	586394.4	6959531.1	0.53	190.9	0.0009
4/30/11 9:35	9/14/11 13:29	137.16	KT2	586408.1	6959604.0	586394.5	6959531.1	0.54	190.6	0.0031
5/3/10 18:50	9/14/11 15:44	498.87	KS2	585829.5	6957249.2	585724.0	6956982.1	0.58	201.6	0.0009
5/1/10 16:38	9/14/11 15:55	500.97	KT3	584823.3	6955102.5	584654.3	6954826.8	0.65	211.5	0.0008
4/29/11 10:48	9/14/11 16:19	138.23	KS3	583631.2	6952755.8	583574.1	6952682.4	0.67	217.9	0.0031
5/2/10 19:37	9/14/11 16:27	499.87	KT4	582440.2	6950375.1	582526.4	6950073.7	0.63	164.0	0.0060
4/28/11 17:15	9/14/11 16:35	138.97	KT4	582448.4	6950375.2	582471.8	6950285.5	0.67	165.4	0.0031
5/2/10 14:57	9/14/11 16:50	500.08	KT5	584248.6	6947092.1	584449.8	6946860.8	0.61	139.0	0.0008
4/28/11 12:47	9/14/11 17:02	139.18	KT5	584253.6	6947084.8	584315.4	6947021.2	0.64	135.8	0.0030